STUDY OF INFRARED EMISSION IN HEATED AIR

ANNUAL REPORT
Subcontroct SD-59-2
By W.H. Wurster ond P.V. Morrone
Report No. QM-1373-A-4
July 1960 - June 1961

CORNELL AERONAUTICAL LABORATORY, INC.
OF CORNELL UNIVERSITY, BUFFALO 21, N. Y.

CORNELL AERONAUTICAL LABORATORY, INC.
Buffalo, New York

Report No. QM-1373-A-4

STUDY OF INFRARED EMISSION IN HEATED AIR

July 1961

ANNUAL REPORT

July 1960 - June 1961

BY: Walter H. Wurster
Walter H. Wurster

APPROVED BY: A. Hertzberg
A. Hertzberg, Head
Aerodynamic Research Dept.

Paul V. Marrone
Paul V. Marrone

THIS REPORT COVERS WORK PERFORMED UNDER BENDIX AVIATION CORPORATION PURCHASE ORDER C 303681 G, SUBCONTRACT SD-59-2 UNDER ARMY ORDNANCE PRIME DA-11-022-ORD-3130.

FOREWORD

This final report presents the results and conclusions of the Study of Infrared Emission in Heated Air carried out by the Aerodynamic Research Department of Cornell Aeronautical Laboratory. The research was supported under Army Ordnance Prime Contract DA-11-022-ORD-3130 by Subcontract SD-59-2, Purchase Order C 303681 G, from the Bendix Aviation Corporation. It is the fourth report on this program, having been preceded by CAL Report Numbers QM-1373-A-1, QM-1373-A-2, and QM-1373-A-3, with the same title. It is understood that this research is to be continued under the direct sponsorship of ARGMA.

The relationship of the radiation measurements contained herein to re-entry has been reported in the Proceedings of the recent AMRAC meeting in Denver, Colorado, May 1961.

ABSTRACT

This report presents the results of a research program whose objective is to formulate a comprehensive picture of the radiation from re-entry bodies. The program is divided into two phases: the experimental determination of the radiative properties of the optically-active gaseous species, and the analysis of the blunt-body flow field, in which the finite rate chemistry of the air is coupled with the aerodynamics of the flow.

Two particular radiating systems were studied, and the results are reported herein. Measurements have been completed on the continuum radiation from the recombination reaction $NO + O \xrightarrow{k_a} NO_2 + h\nu$ in the wavelength range 0.5 to 1.0 microns. The value of the rate constant at 3750°K, $k_a = 4.4 \times 10^5$ cm^3 mole^{-1} sec^{-1}, is some 20 times lower than that measured at room temperature. The spectral intensity of this radiation is presented.

The spectrum of the first positive band system of nitrogen between 0.7 and 1.5 microns has been obtained. Absolute intensities are presented for a range of temperatures and densities. The temperature-dependence of the radiation is shown to be in good agreement with predicted values. The results of this work are compared with those of Keck, et al (Annals of Physics 7, 1, (1959)) which were based on measurements made in air. The measured intensities from pure nitrogen are shown to be less by a factor of five.

The solution for the inviscid, nonequilibrium flow around blunt axisymmetric bodies (i.e. the bow shock solution) has been programmed for an IBM-704 computer. In addition, a similar finite-rate normal-shock solution has been

programmed to study the overall characteristics of the relaxation process behind shock waves. The thermodynamics and chemical kinetics included in the numerical solutions are discussed. Typical results obtained from the normal shock program are presented.

Two bow-shock solutions are presented: a typical high-altitude re-entry condition (i. e. M = 22 at 200, 000 feet altitude) and a hypersonic tunnel test configuration. The rapid expansion of the flow from a high-temperature reservoir in hypersonic test facilities may introduce nonequilibrium phenomena in the expansion nozzle. These effects will, in turn, have an influence on the shock layer around a model in the expanded flow. A finite-rate expansion solution, developed at Cornell Aeronautical Laboratory, was used to obtain the expanded flow conditions. These nonequilibrium results were then used as inputs to the bow shock solution. For both cases, the calculation was carried approximately 65° off the centerline and the computed body shapes closely resembled a circle. The results for the re-entry case indicate the entire shock layer to be in a state of nonequilibrium at a high translational temperature. Results for both examples are presented in graphical form and are discussed in detail.

TABLE OF CONTENTS

TABLE OF CONTENTS (CONT)

INTRODUCTION

The purpose of this research is to obtain a comprehensive and quantitative understanding of the infrared radiation from the heated air surrounding re-entry bodies. The program involves the detailed spectral measurements of the pertinent radiating species and an analysis of the aerodynamic flow field around the body. This analysis takes into account the finite-rate chemistry of the heated air, and provides the concentration profiles of the gaseous constituents and the local thermodynamic properties in the flow field.

Three earlier progress reports[1-3] contain details concerning the subdivision of the overall project into its respective phases, the considerations which have determined the method of attack on each phase, and a description of the equipment involved on all phases. Consequently, these items will be discussed here only to an extent consistent with general completeness.

The program has been divided into two areas. The first involves quantitative measurements on the system of radiating species of air at elevated temperatures; a machine computation of the state of the air in the flow field surrounding the re-entry bodies constitutes the second phase. The combination of these two phases will allow the composite radiation picture to be calculated for re-entry systems. A portion of the second phase involves the study of the chemical kinetic rates necessary to couple the complex chemistry of the heated air with the aerodynamic flow problem.

The question of the applicability of these results to nonequilibrium flow configurations warrants a brief discussion. The results of the flow-field analysis presented in Section II of this report show, for example, that the gases in the entire region between the bow shock and the blunt body may be in a nonequilibrium distribution. This is to say that the concentrations of the various species which make up the heated air are not those which would be obtained from a chemical-equilibrium analysis at the local temperature. This is due to the finite rate at which the reactions occur in the flow. However, given the species concentrations and the degree of excitation of the molecules, the prediction of the spectral radiation can still be reliably made if the transition probabilities for the pertinent transitions of the optically-active molecules are known. These considerations gave rise to the basic approach made upon the problem, which renders the solution applicable to the nonequilibrium problem.

This research does not at present treat the case of nonequilibrium radiation arising from those species formed within the shock front in high-energy states. A general experimental approach to that case cannot be simply made, since a complete duplication of ambient conditions of density, composition, and velocities are required. That problem will receive special attention in later phases of the work.

Section I of this report deals with the radiation phase of the program. Experimental studies were performed on two separate problems involving radiation from heated air. One was the continuum radiation associated with the recombination of NO and O atoms into NO_2. This continuum extends from about 4000 Angstroms to 1.5 microns in the near infrared. Previously reported measurements[4-7] were confined to the visible region of the spectrum, and the

measured rate constants were obtained at room temperatures. The experiments reported herein were designed to measure the absolute intensity of the radiation in the near infrared, and to obtain a rate constant for the recombination reaction which applies at high temperatures ($\sim$ 3000°K).

The second problem was the measurement of the absolute intensity of radiation from nitrogen at high temperatures. The first positive band system in the spectrum of nitrogen extends from the visible through the near infrared. In this wavelength region, it is the strongest of the radiating species in heated air. The spectra of nitrogen over a range of temperature and density are presented. The method of data reduction are also described and the results are discussed.

Section II discusses the machine computation programs used to calculate the state of the gas surrounding re-entry bodies and behind normal shock waves. A general discussion of the thermodynamics and chemistry involved in the programs is presented. The finite-rate, normal-shock solution has been completely programmed for an IBM-704 computer, and has a capacity for 20 species, 40 chemical reactions. A great variety of test cases have been run. Results are presented for a typical air calculation using a seven-species, six-reaction kinetic model. The effect of coupling the degree of vibrational excitation with the chemical reactions is shown.

The inviscid bow-shock problem, employing the inverse method of solution, has been programmed for the 704 computer, utilizing the large-capacity, high-speed core storage unit. At the present time, this program has a capacity for 10 species and 20 chemical reactions. Several test cases have been completed with this program, for both a diatomic gas and air. Results for

a typical re-entry vehicle at an altitude of 200,000 feet and a hypersonic tunnel configuration are presented, using the same air model employed in the normal shock solution.

It is known that viscous phenomena may effect the flow field around a re-entry body in a rarefied atmosphere. However, the viscous effect is not important at the outer portion of the shock layer for altitudes of approximately 200,000 feet and below. The ratio of boundary-layer thickness to shock-layer thickness at the stagnation region of hypersonic vehicles is about one-tenth at this upper altitude. Thus, the inviscid computation can be used with some degree of confidence to predict the chemistry of the shock layer at an altitude of 200,000 feet.

SECTION I - RADIATION MEASUREMENTS PHASE

The need for the study of the individual components in the determination of the radiative properties of a multicomponent gaseous mixture such as air at elevated temperatures has been stressed in the previous progress reports [2, 3]. Because the concentrations of the radiating species each vary markedly and uniquely with changes in the temperature and density of the gas, a prediction of the radiation from the composite gas under arbitrary conditions requires a knowledge of the detailed radiative behavior of each component. Therefore, our purpose has been to assemble the necessary apparatus and to perform detailed measurements of the radiation spectra in order to enable the transition probabilities for the components to be deduced.

The use of the shock tube as a means for heating gases for quantitative spectroscopic studies has become widespread[8, 9], and stems from the distinct advantage that gases so treated are brought to thermodynamic equilibrium at conditions otherwise unattainable in the laboratory. The price for this advantage lies in the extremely short testing times during which the heated gas can be studied; hence, there is imposed the requirement for high-speed spectroscopic equipment.

Complete discussions of the criteria to be met by both shock tubes and spectrographs for the experiments of this research program have been presented in References 1 through 3. In these reports the details of the completed shock tube and the twelve-channel infrared spectrometer have been presented, as well as the use of this combination in some preliminary measurements of the N_2 first positive band system.

A. THE NO-O RECOMBINATION RADIATION MEASUREMENTS

The history of the problem, some exploratory measurements, and preliminary data were presented in Reference 1, the last Semi-Annual Report. For general completeness some portions of that report will be included in the present discussion.

One of the radiative reactions of interest in moderately heated air (3000-4000°K) is that of the radiative recombination

$$NO + O \xrightarrow{k_a} NO_2 + h\nu$$

The rate constant for this reaction has been reported by Kaufman[5]. It was deduced from measurements of the intensity of the radiation from discharge-generated O combining with NO in a flow tube at room temperature. The reported rate is $k_a = 1.5 \times 10^7$ cm^3 mole^{-1} sec^{-1} with an estimated precision of a factor of five. Another recently reported measurement by Fontijn and Schiff confirm this room-temperature reaction rate to an accuracy of 25%.

Appreciable concentrations of the reactants could be generated in the heated air behind the reflected shock wave in a shock tube, and a measurement of the rate constant could be made at higher temperatures and possibly with greater precision. In addition, the temperature dependence of the rate constant might be deduced.

General Discussion of the Experiments

A description of the general features of the continuum resulting from NO_2 formation has been given recently by Garvin, Gwyn, and Moskowitz [6]. They report a continuum which begins at about 3600A, remains fairly flat between 5500 and 6000A, and drops off toward the infrared. They recorded the

spectrum out to 1 micron, although no intensity measurements were made. Stewart [4] has published a profile of the ultraviolet end of this continuum in arbitrary units. The first quantitative results on the intensity were obtained by Kaufman[5], and more recently by Fontijn and Schiff[7], who measured the spectrum only to 6200A. The sharp cutoff of the continuum radiation at about 3600A from the radiative recombination of NO and O at room temperature has been shown by Stewart [4] to verify Gaydon's analysis of the energy of separation of the NO-O unbound system from the ground state of the NO_2 molecule. In measurements with heated gases it would be expected that the additional kinetic energy of the reactant species would cause a slight shift in the cutoff wavelength into the ultraviolet.

The feasibility of making a quantitative study of this system was investigated. Since these experiments were performed with air, near-maximum radiation should occur at the greatest value of the NO-O concentration product. For air at these conditions, the NO_2 concentration is small ($\sim$ 1 part in 10^4 at 3000°K), and is maintained at its equilibrium values chiefly by the three-body reaction

$$NO + O + M \underset{k'_b}{\overset{k_b}{\rightleftharpoons}} NO_2 + M$$

The rate constant for this reaction, measured at room temperature[10], is $k_b = 2.7 \times 10^{16}$ cm^6 mole^{-2} sec^{-1}. The value of k_a measured at room temperature[5] is 1.5×10^7 cm^3 mole^{-1} sec^{-1}. With these two values, the approximate rate of formation of NO_2 by each of the two reactions can be calculated. Using the equilibrium values[11] for the concentrations of NO and O in high-temperature air, one obtains, at 3000°K

Radiative recombination $\frac{d}{dt}\left[NO_2\right] = 1.3 \times 10^{-5} \left(\rho/\rho_0\right)^{3/2}$ moles cm^{-3} sec^{-1}

Three-body recombination $\frac{d}{dt}\left[NO_2\right] = 1.3 \left(\rho/\rho_0\right)^{5/2}$ moles cm^{-3} sec^{-1}

where the approximate density dependence has been included in the equations. At 4000°K each of the production rates is about ten times faster. Thus, in all cases the three-body rate is about 10^5 times faster than the radiative recombination. The three-body reaction keeps the NO_2 concentration in equilibrium with the NO and O concentration even though the radiation density is far below the blackbody value.

Exploratory Experiments

A Bausch and Lomb large Littrow spectrograph was equipped with an adapter[12] which allows four photomultipliers to be positioned in the focal plane of the spectrograph. The radiation intensity in each channel was displayed and photographed with a conventional oscilloscope-camera system. The wavelengths which were monitored in these tests were at 3630, 4000, 4320, and 5380 Angstroms. These wavelengths include the ultraviolet edge of the NO_2 continuum. The shift of the cutoff wavelength into the ultraviolet should have been readily discerned.

The results of these preliminary experiments showed that a rising spectrum was in fact recorded in the four channels from the shock-heated air.

The wavelength distribution corresponded to the profile that had been reported. However, the use of this ultraviolet-to-green region of the spectrum for quantitative measurements was shown to be impractical in a shock tube analysis. This is due to the fact that at these wavelengths the emission from the Schumann-Runge system of the heated O_2 which is present in the equilibrium sample of heated air in the tube has a sizable contribution. This was determined by making separate runs in pure oxygen under conditions which duplicated the oxygen content in the heated air run. The intensities representing the difference between those of air and pure oxygen had the proper distribution as reported for the NO_2 continuum. It was apparent, however, that the errors involved in such a subtractive procedure precluded exact measurements and also obscured any effect such as shift of cutoff wavelength. Experiments in pure nitrogen revealed a total absence of radiation, thereby eliminating any band system of N_2 or any impurities as contributors to the measured radiation in the air experiments.

Several other experimental schemes were used in further experiments to establish the nature of the spectrum from the heated air. One of these was the use of a Dumont K-1430 phototube and a Wratten cutoff filter without a dispersing element. With this system the total radiation between 0.6 and 1.1 microns was recorded, and the resultant intensity was correlated with the reactant concentrations. It became apparent that to analyze the radiation quantitatively, the intensity would have to be obtained spectrally; i. e., as a function of wavelength. Further, with the entire spectrum mapped for a given set of thermodynamic conditions, an accurate value of the rate constant could be obtained. The infrared ($>$ 1.1 micron) portion of the continuum had never been reported, and since the determination of the rate constant requires the measurement of the total radiation, it was felt that this portion of the spectrum should be examined.

This was conveniently done by making use of the multichannel infrared spectrometer which had already been used in the early N_2 work. A series of experiments showed a slow drop in the intensity of the light at longer wavelengths, which between 1.5 and 1.8 microns decreased to about 10% of its value at 1 micron. It was, however, impractical to proceed with the overall spectrum measurement with this instrument because of its low detector response at 0.6 microns, and because the twelve channels could not be made to subtend more than 0.3 microns at any given setting. It was decided to avoid the procedure of shifting the instrument across the 0.5 to 1.5 micron range, while trying to repeat the shock tube conditions identically for at least three runs. The system to be described was therefore designed and used.

Instrumentation for Total Spectrum Measurement

The windows on both sides of the shock tube were used. One side had the multichannel infrared spectrometer deployed in exactly the same manner as shown in Figures 3 and 5 of Reference 3. The spectrometer was used in first order, and the twelve channels spanned the wavelength range from 0.9 to 1.2 microns. Five of the twelve channels were used in the experiments.

The window on the other side of the tube was viewed by five Dumont K-1430 infrared-sensitive photomultiplier tubes, each of which was equipped with a Bausch and Lomb interference filter and an appropriate Wratten cutoff filter, so that each tube responded to a very narrow wavelength band. The half-widths of the filters ranged between 100 and 240 Angstroms. The filter-photomultiplier combinations were placed so that each of them saw almost the same volume of gas. Each tube subtended a viewing cone defined by an aperture of 1-inch diameter at a distance of about 18 inches from the shock tube window. The five overlapping

cones were contained in an aperture of 2 inches at a distance of 12 inches. This was accomplished by means of a five-sided pyramidal mirror assembly which reflects the total beam into five directions in a radial manner (see Figure 1). The filter-photomultiplier assemblies are mounted on a 14-inch diameter circle. The calibration of this system was accomplished in the same manner as that of the multichannel spectrometer, namely by effectively replacing the image of the shock tube window with that of a calibrated tungsten ribbon-filament.

The five wavelengths chosen for study are given in the following table in addition to those covered by the multichannel spectrometer

Instrument	Wavelength (Microns)
Photomultiplier Ensemble	.542
	.598
	.695
	.798
	.906
Multichannel Infrared Spectrometer	.906
	.955
	1.005
	1.085
	1.190

The .906 micron wavelength was recorded by both systems and served as a crosscheck on the overall calibration accuracy and system response.

Each shock tube run constituted a coverage of the continuum at the nine wavelengths shown. The radiation intensities were displayed as a function of

time at a sweep rate of 20 microseconds/cm. In addition, the dual beam oscilloscope which recorded the .906 micron channel using the two systems was also coupled to another oscilloscope which recorded at a slower rate (200 microseconds/cm) and served to monitor the long-time radiative behavior of the shocked gas. Reflected shock pressures were also recorded to monitor shock tube performance for each run.

The general features of the radiation records included a rise of radiation as the reflected shock wave swept by the cone of gas viewed by the respective channels, followed by a reasonably constant radiation plateau. This constant level of radiation in each channel indicated thermodynamic equilibrium, and constituted the datum for the intensity at that wavelength. After each experiment, the calibration lamp radiation at the prescribed current values was passed through choppers and presented to the detectors. These intensities were also displayed and photographed. Thus, a comparison of the signals from shock tube and lamp yielded absolute values for the intensity of the radiation from the shock-heated gas.

The results of the first experiments with this apparatus were presented and discussed in Reference 1. The experiments were in progress at that time and the results were presented as preliminary. They will be summarized at this point.

Several spectra were obtained which showed in general the form of the NO_2 recombination radiation spectrum. The intensity in the nine channels was reported in watts cm^{-3} $steradian^{-1}$ $micron^{-1}$.

The probable error in the data points due to the readability of the records was about 2%. In addition, the largest difference in the radiation intensity at

.906 micron as recorded by the two separate detecting systems was 7%, while for most runs the agreement was within 3%. This difference was an indication of the precision of the calibration procedure, since both tungsten lamps were calibrated against the same NBS standard lamp. The largest source of error in the results arose from the problem of determining the best time (measured from shock wave reflection) at which to measure the radiation intensity level. Variations between 5% and 10% were sometimes recorded over the testing time interval, and hence gave rise to an uncertainty in the absolute spectral intensity. The general procedure was to record the level of intensity at about 120 to 140 microseconds from the time of shock wave reflection. The reflected shock wave required some 30 microseconds to move through the gas in the field of view, and an additional 100 microseconds was ample time for complete equilibration in the tube. The total testing time, measured by both pressure and radiation channels, ranged between 150 and 300 microseconds.

There were several indications that the origin of the radiation was the NO_2 recombination. Primarily, over a broad range of conditions the radiation intensity could be normalized by the product of the NO and O concentrations. In addition, check runs were made in pure N_2 and O_2. For nitrogen at T=4240°K at 4.25 times normal density, no radiation was recorded in any channel. This indicated that the source of the radiation must be linked with the presence of oxygen, and further, that no radiation shock-tube impurities such as CN are present in these experiments. The air used in the present studies was procured as "dry air" from the Matheson Company. One check on the results at high temperatures was made by performing a run using an air mixed from reagent grade N_2 and O_2. The results were essentially the same, and indicated no noticeable impurities in the dry-air container.

Experiments in which pure oxygen was brought to the same conditions as those of the high-temperature air runs yielded only a very small amount of radiation. It was almost immeasurable, due to the low signal - to - noise ratio. It should be noted that experiments in air and various O_2 - N_2 mixtures have been included in the schedule of studies to be performed directly after the measurements on the N_2 first-positive band system.

Preliminary estimates of the rate constant were made from the data, and revealed that the rate at about 3500°K was some 20 times lower than the room-temperature rate reported by Kaufman[5]. It was noticed in the spectra, however, that at 0.6 microns a large spike of radiation was recorded, for experiments in excess of 4000°K. Because of the likelihood of radiation from sodium at this wavelength it was decided to place the interference filters (which determine the bandpass of the photomultiplier detector channels) at wavelengths which would be free of radiation from such unavoidable impurities as sodium, calcium, and potassium.

The final placement of the filters was determined after first photographing as much of the continuum spectrum as possible. A medium quartz spectrograph (f:10) was used together with Kodak 103-F and I-N spectrographic plates to obtain the spectra shown in Figure 2. The first spectrum is that for air at about 4500°K and 3 times normal density, in which the plate was exposed to the total shock tube radiation phenomenon. This includes not only the radiation from the gas during the "clean" testing time, but also the subsequent radiation, largely from impurities and from the interaction of the hydrogen-driver gas with the heated test air. The prominent OH band at 3064 Angstroms is clearly seen.

The use of a capping shutter[13] which limits the plate exposure only to the radiation from the gas after processing by the reflected shock permitted the second spectrum of Figure 2 to be obtained. The radiation from the Schumann-Runge band system of oxygen can be clearly seen on the plate. The radiation of interest to the present problem extends from about 4000 Angstroms into the infrared. The prominent lines in this region are those of potassium, calcium, and sodium. The unexposed region between 5000 and 5500 Angstroms results from a decrease in the sensitivity of the emulsion. The type F plates were used to examine this region in detail. The last spectrum, together with the other results, show that this radiation does not appear in the spectra of either pure oxygen or nitrogen.

The interference filters were placed in the cleanest portions of this continuum, and were now at the wavelengths: 4750, 5100, 6700, 8100, and 9060A. With this configuration, another series of experiments were performed with air at temperatures between 2800 and 4500°K, and densities between 2 and 20 times normal.

Results

The data from a series of experiments near 3700°K are shown in Figure 3. In this graph the measured intensities at the various wavelengths are plotted against wavelength. The intensity was normalized by the product of the NO and O concentrations:

$$Z^2 X_O X_{NO} \left(\rho/\rho_o \right)^2$$

where Z is the compressibility factor, ρ is the air density, and the X's are mole fractions, obtained from Reference 11. The smooth curve of the graph

between 0.4 and 0.62 microns was taken from the detailed spectrum by Fontijn and Schiff [7], which was reported during the course of the present work. The spectrum was fitted to the data at 0.51 microns.

As can be seen, the agreement with the intensity distribution verifies the recombination radiation as the chief contributor to the recorded spectrum. The experiments covered a range of 3 in the factor $Z^2 X_{NO} X_O (\rho/\rho_0)^2$ and the intensities are proportional to it to within 20%.

The rate constant derived from these data at 3750°K for the reaction

$$NO + O \xrightarrow{k_a} NO_2 + h\nu$$

is equal to 4.4×10^5 cm^3 mole^{-1} sec^{-1} ±25%. This is about 20 times smaller than the room-temperature value.

The reaction rate measured at 3750°K is lower than that reported for 300°K by a factor of about $(3750/300)^{-1.2}$, which is reasonable for the temperature variation of recombination reactions. However, between 3000 and 3750°K the values show a $T^{-3.5}$ dependence. This variation cannot reasonably be attributed to a change in the reaction rate constant, but rather, indicates a contribution of radiation from another source at these lower temperatures.

In contrast with the room-temperature work, for air in equilibrium at these conditions, radiation can arise both from the NO-O recombination and from excited states of equilibrated NO_2 molecules. The density dependence of the radiation from these two sources is the same. However, the equilibrium population of the NO_2 falls rapidly to a negligible value by 3750°K[14]. Further, subtraction of the NO-O recombination intensity at the lower temperatures (based on a $T^{-1.5}$ dependence) leaves a residue which is consistent with the radiation

from NO_2 based on estimates made from the absorption coefficient of the NO_2 molecule. A recent paper by Broida and Schiff and Sugden [15] shows a structured spectrum at the cutoff of the room temperature NO-O recombination continuum which suggests the presence of excited NO_2 molecules in their experiments. The precision of our data does not warrant further analysis of the NO_2 contribution.

One experiment was performed at 2800°K. At these temperatures the radiation was seen to rise gradually in time to an equilibrium value (for higher temperatures the rate of rise was due only to the transit time of the reflected shock wave across the viewing port). The rate was strongly suggestive of the relaxation time to chemical equilibrium. A check was made on the kinetics of this shock tube run by using the normal shock program discussed in Section II of this report. These results gave good agreement between the measured rise of the radiation and the formation of NO molecules which is rate-determining for NO_2 formation. This experiment, coupled with the absence of radiation in pure N_2 or O_2 experiments serve to confirm the source of the radiation and the validity of the results.

B. THE NITROGEN INFRARED MEASUREMENTS

One of the principal radiating species in heated air is the nitrogen molecule, whose first positive band system extends from the visible to about two microns in the infrared. The only reported transition probabilities for this system were deduced from a few broad-band measurements made in heated air [9]. The need for a detailed study of this system was clear, and thus it became a primary aim of the present research program.

Description of the Experiment

The apparatus for these experiments consists basically of the shock tube, used to process the gas, and the twelve-channel infrared spectrometer, with which the absolute intensity of the spectrum of the gas was measured. The criteria leading to the design of these components together with the details of construction and calibration have been reported in References 2 and 3. Briefly, the shock tube has a test section 30 feet long, of 3-inch inside diameter. It is equipped with contoured, sapphire windows near the reflecting wall. It is designed for operation at high driver-gas pressures (30,000 psi) and at good purity levels (total rate of rise at vacuum ~ 2 microns/hr.). Combustion drive was not used because of the inherent difficulties of performance and cleanliness with combustion-driven shock tubes.

The twelve-channel infrared spectrometer was designed to span the range from 0.7 to 2.4 microns. It is an f/3.5 Ebert-type grating instrument and the twelve channels subtend about 0.3 microns in first order, with a bandpass of 0.01 microns per channel, each of which has a lead selenide detector with about 10 microsecond response time.

The use of this system and some preliminary measurements of the nitrogen system has been reported in Reference 3. Since that time the system has been modified and refined, particularly in regard to the radiation calibration techniques and to actual shock tube operation. These will be described in the next subsection.

Experimental Procedure

The shock tube was thoroughly scrubbed with alcohol and hard-pumped between runs. Prepurified nitrogen from the Matheson Company was used for the

experiments. The following mass-spectrometer analysis of the nitrogen was obtained from the Matheson Company:

O_2	5 ppm
H_2O	3 ppm
Hydrocarbons	less than 0.5 ppm .
CO_2	non-detectable
CO	non-detectable
H_2	non-detectable

The gas was used with no further processing. Initial test gas pressures were read on a manifold of Wallace and Tiernan absolute pressure gauges, which were calibrated and cross-checked with each other. The speed of the incident shock wave was measured with thin-film ionization gauges at four intervals in the last six feet of the shock tube. The intervals are 18 inches apart and the elapsed time was measured with a digitalized output unit to the nearest microsecond.

In order to traverse a spectrum from 0.7 to 1.2 microns in the second order (which was done in these experiments), the conditions of the gas must be reproduced exactly for five to six shock tube runs. Using only pressure breaks on the diaphragms at the 2500 psi level makes this almost impossible, due to the unavoidable variations in the diaphragms. This problem was overcome through the use of a double-diaphragm technique. The double diaphragm unit consists of two diaphragms separated by a 3-inch spacer. During the loading process, this small chamber is automatically maintained at one-half the driver-gas pressure. For desired operation at 2500 psi, the chamber contains 1250 psi. Since the driven section is at a comparative vacuum (10-200 mm Hg), the diaphragms

support a pressure differential of 1250 psi. Upon venting the chamber, the full 2500 psi bears first upon the diaphragm closest to the driver, and, when it ruptures, upon the second. Thus, the only requirement upon the diaphragms is that they support 1250 psi, and break at less than 2500 psi. This is easily accomplished, since normal variations in the rupture pressure of the diaphragms are less than $\pm$ 200 psi. With this system a series of runs can be made, in which the wave speed in any of the timing intervals is duplicated to within 1 microsecond out of 150. This reproducibility is within the error in the determination of the density and temperature behind the reflected shock. Thus the data require no corrective normalization between successive experiments in a given series at constant reflected-shock conditions.

The absolute intensity calibration of the spectrometer was carried out in the following manner. During the shock tube run, the entrance slit (1 x 12 mm) of the spectrometer is focused on the sapphire window of the shock tube. After the run, it is focused onto the tungsten ribbon filament of a standard lamp. This is done without changing the optical geometry. A fast chopper is employed to produce a square wave output which is recorded by each channel. Thus the primary data consist of two records which are the ratio of the radiation from the gas and from the tungsten lamp.

The voltage output of a typical channel is shown in the following sketch:

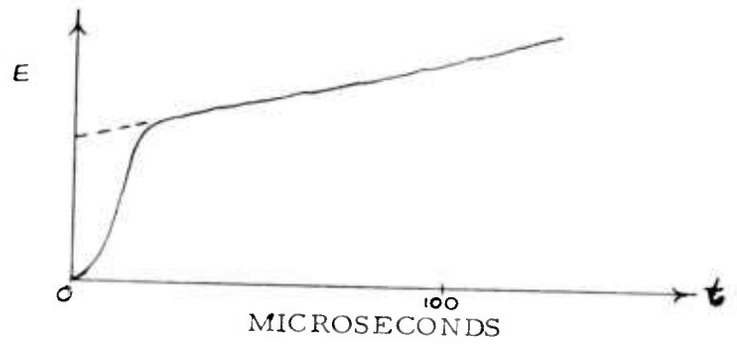

The sharp rise of the signal corresponds to the transit time of the reflected shock wave through the subtended volume of the test gas. A rather linear rise in signal follows, and corresponds to a radiation increase which is felt to be due to a small rise in the temperature of the gas in the tube. The radiation is highly temperature dependent, and the temperature rise needed for this increase is too small to be correlated with the reflected shock pressure, whose output over the total interval remained constant. The datum for each channel was taken to be the intercept of the linearly extrapolated slope at $t = 0$, where the temperature would be that calculated by simple shock tube theory.

The working standard lamps were obtained by comparison with a National Bureau of Standards Lamp whose output was measured and certified at NBS. The comparison was made over a broad range of wavelengths from 0.5 to 2.4 microns by alternately passing the radiation from the NBS lamp and the working standard lamps into a Gaertner monochromator. The current in the NBS lamp was provided by a stabilized power supply which was operated from an 0.01% line regulator. The current was set at the NBS value with an 0.25% Weston 370 ammeter. Storage batteries were used to power the working standard lamp, and an 0.5% ammeter was used both for the calibration and subsequent operation of the lamp in the experiments. Thus, the accuracy of this meter did not enter into the calibration. Both lead sulphide and infrared-sensititve photomultiplier tubes were used in the calibration to maintain the highest signal-to-noise ratios and to minimize the reading error in the comparison of output signals from the lamps. Overall-system linearity was checked by comparing the readings for the NBS lamp radiance at 25 and 30 amperes, since the NBS lamp was calibrated at both current values. The effect of aging of the lamps was studied, and the determina-

tion of the usable working areas of the filaments was made by measuring the radiance gradients along the filaments.

The accuracy of the overall calibration of the working standard is felt to be better than 5%. The largest error in the absolute values used in the experiments is that reported for the NBS lamp itself[16].

The spectrometer was checked out to insure that no radiation from unwanted orders or wavelengths were overlapping the detectors at any given setting. Use was made of silicon windows, water cells, Kodak infrared filters and several organic liquid cells in these checkouts and in the runs where necessary. In general, only the radiation subtended by the detector array was permitted to enter the spectrometer. The intensity calibrations were always made with the order-sorting filters in the system.

The linearity of the detecting system was also checked by separately verifying the linearity of the electronic system of amplifiers and by an inverse-square experiment, where the response of the detectors was measured as a function of the distance from a point source. No deviation from linearity was noted for values of detector output which greatly exceeded those obtained in the experiments.

Results

An exploratory series of runs using the multichannel spectrometer in first order revealed that the prominent features of the spectrum lay between the low wavelength limit of 0.7 microns and about 1.5 microns. This region of the spectrum was then carefully surveyed in second order, by making a series of runs at conditions of constant temperature and density. The resultant spectrum is shown in Figure 4, where the radiation is plotted in watts cm^{-3} $steradian^{-1}$

micron^{-1}. The twelve data points from a single run are shown as separate symbols, and the precision in the data can be determined by examining the spread in intensity at a given wavelength for a number of overlapping runs. Also plotted along the abscissa are the pertinent band-head positions according to Dieke and Heath[17], with the heights of the markers scaled to the values of the overlap integrals after Jarmain and Nicholls[18]. The vibrational band sequences can be clearly seen, and indicate the advantages of the multichannel approach, in that all radiation corresponding to a given symbol on the plot was recorded from the same sample of gas.

The radiation from the standard lamp is given in units of watts cm^{-2} steradian^{-1} micron^{-1}. Conversion to the units plotted is accomplished by dividing by the path length through the radiating gas, equal to the inside diameter of the shock tube (7.60 cm was used). The sapphire window-transmission correction was taken to be 0.9, and finally, the data were corrected by a factor of 1.4 to account for the effect of reflections inside the shock tube. This factor was obtained by experiments described in the Appendix. Thus, the intensity plotted in Figure 4 was directly obtained from the data by the relation

$$I\left(\frac{\text{watts}}{\text{cm}^3 - \text{ster-micron}}\right) = \frac{I'}{(7.6)(.9)(1.4)}\left(\frac{\text{watts}}{\text{cm}^2\text{-ster-micron}}\right)$$

In Figure 5 are presented several spectra spanning one of the vibrational band sequences ($v' = 1$, $v''=0$) of this first positive system ($B^3\Pi \longrightarrow A^3\Sigma$) between 0.78 and 0.91 microns. These spectra were obtained by varying the density and temperature of the nitrogen in experiments with a constant wavelength setting of the spectrometer. The essential features of the spectrum are the same,

and the variation in intensity results from the change in the population of the upper energy level involved in the transitions. This effect is more clearly seen in Figure 6, which gives the temperature dependence of the radiation. Considering the radiation to arise from an upper level of energy E', the intensity is proportional with the population in this level:

$$I = c \frac{n}{L_o} \frac{e^{-E/kT}}{Q_{N_2}}$$

where n is the number of N_2 molecules per cm^3, L_o the Loschmidt number, and c is a constant. Q_{N_2} is the internal partition function for nitrogen. It is plotted in Figure 7, and was obtained from Reference 11. Dividing and taking the logarithm, one obtains

$$\ln \frac{\left(I Q_{N_2}\right)}{\left(n/L\right)} = - \frac{E}{k} \left(\frac{1}{T}\right) + \ln c$$

Thus, a plot of the left side vs. $1/T$ should yield a straight line, whose slope is $-E/k$, and whose intercept permits the constant c to be evaluated. Eight temperatures between 6000 and 7200°K are plotted for each of two wavelengths, chosen at each edge of the recorded band sequence. It can be seen that a good straight line can be passed through the points. The slope of the line at 0.887 microns which contains the head of the (1, 0) band corresponds to $E = 58800\ cm^{-1}$. This is in very good agreement with the best reported value of $61700\ cm^{-1}$, and substantiates the radiation origin to be N_2. Keck et al[9] have reported the f number for this band system in nitrogen to be 0.025. The results of the present work are a factor of five below their value. This

discrepancy is significant and is illustrated in Figure 8. Because their results were deduced from radiation data taken in shock-heated air, the discrepancy may be due to a prominent radiator present in air but not in nitrogen. This point was checked by repeating the 0.78 and 0.91 micron experiment with air at T = 5400°K and a density of 0.9 times normal. The resultant radiation was normalized to the amount of molecular nitrogen present in the air at these conditions. At 0.8 microns the radiation intensity was equal to that predicted by the present pure-nitrogen work, indicating the absence of other radiation species in this wavelength region, at least for temperatures below 6000°K. Thus it is felt that the lower intensity values for the nitrogen spectrum measured in these studies are valid.

The spectral resolution of the data allows the transition probabilities to be determined with good precision. Because this analysis is presently being made, it could not be included in this report, but will be submitted for publication shortly. Based on the calculations of Keck, et al, the f number should be about 0.005, one-fifth of their reported value.

C. SUMMARY AND CONCLUDING REMARKS - RADIATION PHASE

1. The reaction rate constant for the NO-O radiative recombination

$$NO + O \xrightarrow{k_a} NO_2 + h\nu$$

has been measured to be 4.4×10^5 cm^3 $mole^{-1}$ sec^{-1} $\pm 25\%$ at temperatures of 3750°K. This rate is 20 times smaller than that reported for this reaction at room temperature.

2. At lower temperatures (2800-3100°K) additional radiation was recorded and is attributed to the bound states of thermally equilibrated NO_2.

3. The detailed and intensity-calibrated spectrum of the first positive band system of nitrogen has been obtained between 0.74 and 1.2 microns for a range of temperatures between 5800 and 7200°K. The observed temperature dependence of the radiation is in good agreement with equilibrium-radiation theory and clearly identifies nitrogen as the radiating gas.

4. The intensity of the radiation from pure nitrogen is lower than previously reported values [9] by a factor of five.

The scope of the continuing research in this area includes the experimental determination of the other contributors to the radiation from heated air. These are presently felt to be the continuum radiation [19] arising from the interaction of electrons with the atoms and molecules of the heated air. It is planned to study the radiation for a broad range of N_2 - O_2 ratios, from which the effectiveness of the various scatterers may be deduced.

SECTION II - RE-ENTRY BODY FLOW FIELD ANALYSIS PHASE

The solution of the inviscid nonequilibrium blunt-body problem (which has been discussed previously in References 1, 2 and 3) is needed to predict the time history of radiation from the hot gas surrounding a re-entry vehicle. The present analysis is based on the inverse method of solution (i. e. the shock shape and size is prescribed) and employs coupled vibration-dissociation reactions to describe the thermochemical state of the gas behind the bow shock wave. This general bow shock problem has been programmed for an IBM-704 computer. In addition, a similar finite-rate solution has been programmed for normal shock waves to assess the variation of rate constants on the over-all relaxation zone. A general description of both programs and pertinent results obtained to date will be discussed.

It is known that the flow field around a re-entry vehicle in a rarefied atmosphere may be influenced by viscous effects. Cheng[20] defines a flow regime where boundary layer or vorticity interaction theories may apply as $O(1) \leq \varepsilon K^2 < \infty$ where ε is the inverse density ratio over the shock. K^2 can be approximated by

$$K^2 \approx \frac{\varepsilon A}{\lambda_\infty}$$

where A is the body nose radius and λ_∞ is the mean free path upstream of the shock. For a typical re-entry vehicle (i. e. one foot nose diameter), at an altitude of 200,000 feet, $\varepsilon K^2 \approx 500$. However, this parameter is about 50, or approaching $O(1)$ at 250,000 feet. Scala's[21] similar results show the ratio of boundary layer thickness to shock layer thickness in the stagnation region of hypersonic vehicles

is about 1/10 at 200,000 feet, and increases to 1/2 at 250,000 feet altitude. The inviscid solution can be used with some degree of confidence to predict the chemistry of the shock layer at 200,000 feet.

A. NORMAL SHOCK SOLUTION

General Discussion

The normal shock program is similar to the bow shock problem in the numerical aspects of the solution, and is identical with respect to the thermodynamics and chemistry. Since it is a much less complex program than the bow shock solution, the general characteristics of relaxation phenomena behind shock waves can most easily be discussed in terms of the normal-shock solution. Consider the sketch:

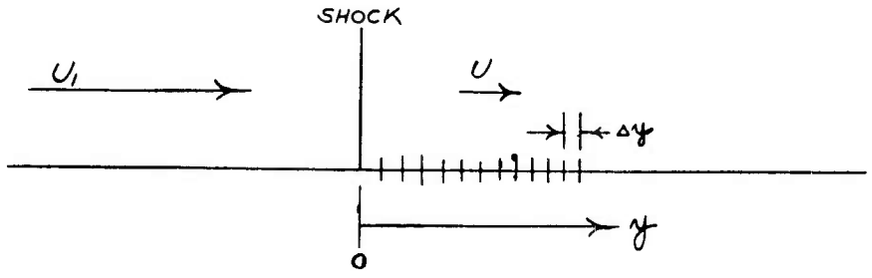

In shock coordinates, the flow is advancing into the shock wave at velocity U_1 and leaving at velocity U. When the air passes through the shock wave, it is compressed and most of the kinetic energy available in the free stream is converted to thermal energy. The active (i.e. translation, rotation) contributions to the internal energy of the gas are very quickly adjusted to the equilibrium values in the time of a few molecular collisions. However, the nonactive degrees of

freedom (i.e. vibration, dissociation and ionization) adjust much more slowly. Duff[22] has investigated the chemical dissociation-recombination process behind normal shocks in air considering vibrational equilibrium of the diatomic species. The addition of vibrationally nonequilibrated diatomic species and the coupling of this vibrational relaxation process with the chemistry has been studied by Teare.[23]

The mathematical description of this relaxation process used in the CAL program is obtained from the solution of a set of simultaneous differential equations to obtain the density (ρ), pressure (p), flow velocity (U), concentration of the j^{th} species (γ_j) and vibrational energy of the j^{th} species (ε_j) at any distance (y) behind the shock wave. (Detailed analyses of the normal and bow shock problems can be found in References 2 and 3 and will not be presented here.) The conditions immediately behind the shock wave can be determined in a number of ways, depending on the thermochemical description of the problem. In general, each species (M_j) is described thermodynamically with translation, rotation, vibration (described by harmonic oscillator relations for diatomic species), and excited electronic states contributing to the internal energy. The translational, rotational and electronic states are assumed to equilibrate immediately behind the shock and determine the initial nonequilibrium temperature. In flow regimes where the vibrational relaxation time for the diatomic species is much less than the chemical or ionization relaxation times, the diatomic species can be assumed to be equilibrated vibrationally with the three preceding degrees of freedom. However, for low-density regimes, vibrational relaxation times become long, and the diatomic species will be in a state of vibrational nonequilibrium immediately behind the shock. This is

described through a system of harmonic oscillators that relax to equilibrium conditions while maintaining a Boltzmann distribution about a vibrational temperature (T_{vj}).

Since dissociation can proceed from any vibrational level, the assumption of vibrational equilibrium immediately behind the shock leads to a greater population of higher energy levels, and to a higher rate of dissociation. For the flow conditions where vibrational nonequilibrium is important, only the lowest vibrational levels of the molecules are populated, so that dissociation will proceed more slowly than if vibrational equilibrium were established. In these regimes, coupling the dissociation rate constant to the degree of vibrational excitation is a more accurate description of the relaxation phenomenon. This slows down the dissociation process and a higher temperature is maintained during the period of vibrational relaxation than if the vibration and dissociation proceeded independently.

Discussion of Program and Results

The normal shock program has been completed for the IBM-704 computer, and has been used to investigate relaxation phenomena in a variety of gases. A capacity of 20 species and 40 chemical reactions has been included in the program. In addition, the thermodynamic description of each species has been improved over that discussed in Reference 1. Higher electronic states are now included, with a capacity of eight electronic levels for each species, adding considerably to the accuracy of the solution. A variable Δy interval is employed in the step-by-step integration procedure away from the shock. In this process, the interval is doubled after a specified number of successful steps (provided certain tests are passed, i.e. per cent change in T, change in species concentration,

etc. are within given bounds) until a maximum specified interval size is reached. If changes in an interval are too large, the interval size is decreased until all tests are passed. Small intervals are then used in regions of rapidly changing variables (i.e. near the shock front), while progressively larger intervals are used as the variables asymptotically approach equilibrium values.

The results of a typical normal shock computation are shown in Figures 10 through 12. For this particular case, vibrational equilibrium immediately behind the shock was assumed. The initial conditions of p = 1 mm Hg and shock Mach number of 12.3 are from a typical shock tube test. Figure 10 shows the species distribution as a function of distance behind the shock wave. Seven species (O_2, N_2, O, N, NO, NO^+, e^-) were taken to define the air kinetic model and the following six reactions were used: ($k_{F_i\infty}$ denotes the forward rate at vibrational equilibrium, in cm^3/mole-sec):

1. $O_2 + M \rightleftharpoons 2O + M$ $\qquad k_{F_{1\infty}} = 1.1 \times 10^{25} (T)^{-2.5} \exp\left[\frac{-59380}{T}\right]$

2. $N_2 + M \rightleftharpoons 2N + M$ $\qquad k_{F_{2\infty}} = 6.3 \times 10^{23} (T)^{-2} \exp\left[\frac{-115129}{T}\right]$

3. $NO + M \rightleftharpoons N + O + M$ $\qquad k_{F_{3\infty}} = 1.5 \times 10^{21} (T)^{-1.5} \exp\left[\frac{-74555}{T}\right]$

4. $O + N_2 \rightleftharpoons NO + N$ $\qquad k_{F_{4\infty}} = 5.5 \times 10^{11} (T)^{0.5} \exp\left[\frac{-36245}{T}\right]$

5. $N + O_2 \rightleftharpoons NO + O$ $\qquad k_{F_{5\infty}} = 1 \times 10^{12} (T)^{0.5} \exp\left[\frac{-3121}{T}\right]$

6. $N + O \rightleftharpoons NO^+ + e^-$ $\qquad k_{F_{6\infty}} = 5 \times 10^{13} (T)^{-0.5} \exp\left[\frac{-31715}{T}\right]$

The formation of atomic species (O and N) is seen, with the subsequent decrease in concentration of the original molecular species (O_2 and N_2) as the distance from the shock wave increases. The overshoot in NO concentration, which is typical of chemical relaxation zones in air, reaches a maximum approximately one centimeter behind the shock. A positive gradient in electron concentration exists until 1.5 cm behind the shock, where the maximum electron concentration is reached. At this point, there is a 20% overshoot in the electron concentration over the final equilibrium value. The magnitude of this electron overshoot is dependent on shock Mach number and density, and is as high as a factor of two at the higher shock velocities. It should be noted that equilibrium concentrations are not reached until some 20 cm behind the shock, indicating a long relaxation zone.

It is of interest to note the role each reaction plays in this relaxation process. An insight to this can be seen from Figure 11, where the ratio of total forward rates to reverse rates are given as a function of distance behind the shock. Immediately behind the shock, this ratio is infinite for the dissociation reactions, since the reverse reaction is zero, and the whole process proceeds in the forward direction. At final equilibrium, this ratio would be one. The two-body NO exchange reactions and the ionization reaction reaches local equilibrium much closer to the shock than do the slower dissociation reactions. It is the exchange reactions that produce the NO overshoot, since they tend to put the NO in equilibrium with the molecular O_2 and N_2 early in the relaxation zone. A slight undershoot in the ratio is seen for these reactions indicating that the reverse rate (which deletes NO) is dominant in that regime, and the decrease from the overshoot maximum is aided. Figure 12 shows the effect of the chemical system on the gasdynamic properties of temperature and density.

Immediately behind the shock, the temperature, as determined from translation, rotation, vibration and electronic excitation, is approximately 7200°K. The temperature decreases monotonically through the relaxation region towards the equilibrium value of 4400°K. An increase of approximately 50% is seen in the density ratio during the chemical process. Thus, the early part of the nonequilibrium zone consists of molecular species at extremely high translational temperatures. For very high altitude re-entry, this early part of the relaxation zone may fill the entire shock layer, giving a substantially different flow field than that computed from equilibrium conditions.

Conditions of vibrational nonequilibrium have also been investigated using the normal shock program. In this analysis, the forward rate constant at vibrational equilibrium for the i^{th} reaction ($k_{F_{i\infty}}$) is modified by the vibrational coupling factor V_j through

$$k_{F_i} = k_{F_{i\infty}} V_j^{A_{ij}}$$

A_{ij} can be 1 or 0, denoting that vibrational equilibration will proceed coupled to or independently of the chemical reaction. Since the vibrationally relaxing species are considered to be a system of harmonic oscillators in a Boltzmann distribution about a vibrational temperature, T_{vj} , this T_{vj} will start at the original ambient temperature immediately behind the shock. In general then, at $y = 0$, $T_{vj} \ll T$. This vibrational relaxation can be seen in Figure 13, which shows the temperature distribution behind a Mach 19 shock wave into 100 microns of air. For this case, the degree of vibrational nonequilibrium was coupled to the dissociation reactions, and the same kinetic air model described

previously was used. The temperature (T_2) as determined from translation, rotation and excited electronic levels is approximately 19,000°K at $\eta_f = 0$, and decreases towards the equilibrium value of 6000°K. Both the molecular oxygen and nitrogen vibrational temperatures are 300°K at $\eta_f = 0$ (the original ambient value) and increase towards the translational temperature. Since the oxygen equilibrates more rapidly than the nitrogen, the $T_{V_{O_2}}$ reaches local equilibrium sooner (i.e. $\eta_{f_{eq.}} = .26$ cm for $T_{V_{O_2}}$ as compared to $\eta_{f_{eq.}} = 2.5$ cm for $T_{V_{N_2}}$). Since the translational temperature is decreasing at this point, the vibrational temperature overshoots the local equilibrium value, and approaches the final equilibrium result from above. This phenomenon is more pronounced for $T_{V_{O_2}}$ than for $T_{V_{N_2}}$ since it occurs earlier in the relaxation zone where T is decreasing very rapdily. When $T_{V_j} < T$, $V_j < 1$ and the forward rate constant is reduced, slowing down the rate of formation of the atomic species. However, during the overshoot regime, $V_j > 1$, and the rate constants are enhanced. Since the atomic species O and N are delayed early in the relaxation region, the formation of electrons is also delayed, since it is the recombination of O and N through the sixth reaction that gives rise to the electrons. However, the point of maximum electron concentration is relatively unaffected by this coupling. It is the initial gradient in the electron concentration which is most sensitive to the effect of V_j. In general then, the vibrational coupling phenomenon tends to decrease the dissociation process early in the relaxation zone, keeping the translational temperature high.

Conclusions

The normal shock solution gives a clear picture of the thermochemical phenomena occurring behind shock waves. This solution can be used to gain an

insight into the chemistry of actual shock layers surrounding re-entry vehicles, since it closely resembles the stagnation streamline solution. However, near the body, the actual flow velocity approaches zero along the stagnation streamline. Thus, the ratio of chemical time to particle residence time becomes small, and the process approaches equilibrium much more rapidly near the body than indicated by the normal shock solution.

The normal shock program, then, yields a description of the relaxation zone, showing the species distribution with the typical NO and electron overshoots, the decrease in temperature, increase in density, and the effect of the coupling of vibration with dissociation. This normal-shock solution is now complete for any multicomponent gas mixture of atomic and diatomic molecules and will be used to determine the importance of various rate constants, to aid in the interpretation of shock tube data and give an insight into the nonequilibrium shock layer in the stagnation region of hypervelocity vehicles. The computational time is very short for this program, in that approximately 45 seconds are required to compute the relaxation zone for a single diatomic gas (i.e. pure oxygen), and about 6 minutes to obtain a solution for air using the air model previously discussed.

B. BOW-SHOCK SOLUTION

General Discussion

The thermodynamics and chemistry of this program are identical to those of the normal shock, and the greater complexity arises from a more difficult flow situation. A shock-wave size and shape is specified in the inverse method[24], and the body obtained from mass conservation considerations in the system of equations. Consider the sketch

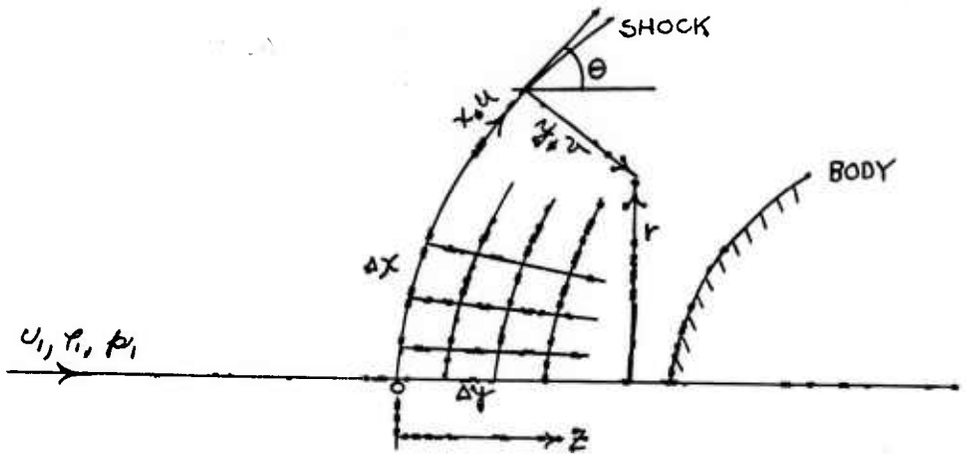

where x is the distance along the shock and y is the coordinate normal to it. The shock is divided into m values of Δx as shown, and the conditions immediately behind the shock at each point are determined from the local normal-shock considerations discussed in the previous section. Once these starting values have been obtained, the entire solution advances forward one interval normal to the shock wave. The solution cannot proceed forward one ray at a time, since the derivatives in the x direction parallel to the shock are needed. These represent the flow swept by a point on any given ray, since the rays do not follow streamlines, but cross them. Accuracy depends on the accuracy with which the x derivatives are known, the size of the mesh intervals, the method of numerical integration, etc.

Discussion of Program and Results

Since the last Semi-Annual Report [1] was completed, the high-speed core storage unit has been installed in the computer, and the bow shock solution has been reprogrammed to take advantage of the larger capacity. At the present time, this solution has a capability for 10 species and 20 chemical reactions, with thermodynamic descriptions identical with those of the normal shock program.

A variable Δy interval has also been incorporated in the body shock program, eliminating the need for an accurate knowledge of the initial Δy step to be used. Subject to the various tests included in the solution, the program selects an initial step size that will satisfy all requirements. Thus, small steps can be taken both near the shock wave and near the body. For the test cases discussed in this report, a three-point fit has been used for the x derivatives. Upon final refinement and completion of the program, a more accurate five- or seven-point fit will be used. The method of computing these derivatives is incorporated in a separate program subroutine that can be easily changed. The programming of the solution is essentially completed, and a number of test cases have been run, both with a diatomic gas (i.e. O_2) and with air.

1. Re-Entry Case

A typical re-entry condition was chosen as the first air-test case, using the same air model previously discussed, with vibrational equilibrium assumed immediately behind the shock wave. A velocity of 23,000 ft/sec at 200,000 ft. altitude was chosen. Using the 1959 ARDC atmosphere, the ambient conditions are

$T_1 = 249.44°K$ $\qquad$ $\rho_1 = 3.1782 \times 10^{-7}$ gm/cc

$P_1 = 2.2281 \times 10^{-4}$ atm $\qquad$ $MW_1 = 28.962$ gm/mole

Figure 14 shows the nose region of the re-entry vehicle, with a catenary shock wave having an approximate 6-inch radius at the centerline specified. The body shape as computed from mass-flow considerations is shown in the shock coordinates in Figure 14a. This plot actually shows how the body pulls away from the shock. A slight waviness can be seen in the body shape, with more pronounced inaccuracies on the end rays. This is due to the fact that a linear fit is presently

used for the χ derivatives on the end rays. These outermost points should be disregarded for the test cases. At the present time, a program stop occurs when the first ray reaches the body (i.e. ray closest to centerline), and the solution is not carried into the body to obtain a more accurate determination of the body shape on the outermost rays. Thus, it is not presently known whether the slight waviness is due to the 3 point χ derivative fit, or to possible inaccuracies in the mass conservation criterion as the distance away from the centerline increases. The entire χ derivative subroutine is now being refined, and this refinement will lead to a more accurate determination of body shapes. In the results presented here, a total of 24 rays (i.e. $\Delta\chi$ divisions) were used in the computation. As shown in the axisymmetric coordinate system in Figure 14b, the body shape closely resembles a circle. The shock standoff distance is seen to lie between the computed equilibrium and frozen values, which were obtained using the relation of Li and Geiger[25]. The present solution was carried to approximately 60° off the centerline, requiring a computing time of one hour and fifteen minutes.

Figure 15 shows the temperature distribution in the shock layer along 4 rays labeled in Figure 14b. The temperature immediately behind the shock as determined from translation, rotation, vibrational excitation and higher electronic levels is approximately 17,500°K along a ray near the centerline (i.e. χ = .06 is about 3° off the centerline). However, the temperature at ψ = 0 at approximately 50° off the centerline (i.e. χ = .86) is much less, 11,000°K. The most pronounced changes in the temperature occur near the stagnation region (χ = .06) since the reactions progress rapidly here due to the high temperature and density and because the local flow velocity is low. It is seen that the entire shock layer

is in a state of nonequilibrium, at temperatures greatly in excess of the equilibrium normal-shock result ($\sim$ 6200°K).

Figures 16, 17, and 18 show the species distributions in the shock layer around the nose cap of the vehicle. The equilibrium normal shock results are given as a reference on each figure. These figures should be interpreted as giving the species concentration along a ray from the shock ($\psi = 0$) to the body, i.e. walking along the ray normal to the shock until the body is reached. The electron concentration (Figure 16) shows an extreme gradient from the shock to the body, with an overshoot of some 70% over the equilibrium value for the ray closest to the centerline. However, along an outer ray ($\chi = .86$) the electron concentration is an order of magnitude less than the value near the stagnation region. The electron concentration gradient will have a strong influence not only on gaseous radiation calculations, but also in the determination of radar cross-sections.

The chemical species distribution is shown in Figures 17 and 18, and it is interesting to note extreme overshoot in NO concentration above the equilibrium normal shock solution (approximately two orders of magnitude). This overshoot occurs on all rays, denoting that the entire shock layer has an extremely high concentration of nitric oxide at the high nonequilibrium temperatures discussed previously. The oxygen and nitrogen atomic species are seen to approach equilibrium values within the shock layer. However, the small oxygen molecular species concentration is still an order of magnitude above the normal shock value when the body is reached. Thus, for this typical re-entry case, the front portion of the shock layer is in a state of nonequilibrium with large amounts of NO and O_2 at extremely high temperatures. This will give a considerably different radiation picture than than computed from equilibrium conditions (i.e. $T \gtrsim 6000°K$, with small amounts of NO and O_2).

2. Hypersonic Tunnel Case

The rapid expansion of the flow from a high temperature reservoir in hypersonic test facilities may introduce nonequilibrium phenomena in the expansion nozzle. These effects will, in turn, have an influence on the shock layer around a model in the expanded flow. Thus, it is necessary to obtain a complete flow solution for the tunnel-model configuration. Using conditions similar to those encountered in hypersonic tunnel investigations (i.e. reservoir pressure= 100 atm., reservoir temperature = 6000°K), the finite-rate expansion was computed using a program recently developed at Cornell[26]. The resultant nonequilibrium flow conditions were used as inputs to the bow shock program. The results chosen as test section conditions were:

$T_1 = 132°K$ $\quad [O] = .158$ moles/orig. mole $\quad [N_2] = .689$

$p_1 = 2.5 \times 10^{-5}$ atm $\quad [N] = 1.5 \times 10^{-10}$ $\quad [NO] = .06$

$A/A^* = 18,190$ $\quad [O_2] = .084$ $\quad [Ar] = 8.6 \times 10^{-3}$

$u_1 = 4.2 \times 10^5$ cm/sec.

Thus, the ambient conditions consisted of large amounts of O and NO indicating freezing of these species early in the expansion process. Again, a catenary shock shape was assumed, having a radius at the centerline of approximately 6 inches. This would presume, then, a six-inch nose radius model in the nozzle test section. As in the previous test case, the model shape closely resembled a circle.

Figure 19 shows the temperature distribution in the shock layer. There is a marked difference in this distribution from that calculated for the 200,000 ft. re-entry case. This is due to the low density in the test section (i. e. typical

of approximately 250,000 ft. altitude) giving longer relaxation times, and to the presence of large amounts of O and NO in the flow. For the innermost ray (χ = .12) the temperature stays practically constant and does not start to decrease toward an equilibrium value until the vicinity of the body. Along the outer rays, the temperature increases slightly, similar to an isentropic compression for the ideal gas case, before the chemistry begins to decrease it. For the outermost ray, this latter effect is unnoticeable up to the point where the body is reached.

This pronounced effect is illustrated in Figures 20, 21, and 22, which show the species distribution in the shock layer. The ambient oxygen atom concentration, which is about a factor of three below the final equilibrium normal shock value exists along all rays well into the shock layer, before an increase in this concentration occurs, first along the ray nearest the centerline. However, the body is reached well before the equilibrium value is attained. The initial NO concentration fills the entire shock layer, and begins to increase in the typical overshoot manner. It is seen that the body is reached well before the maximum in this overshoot occurs, leaving the shock layer with an NO concentration some two orders of magnitude greater than the equilibrium normal shock value. The N atom concentration resembles the previous case, since the ambient value of N is practically zero (i.e. $(N)_{amb.} \approx 10^{-10}$ moles/orig. mole). Figure 22 shows the electron distribution around the model nose cap. It is seen that the body is reached well before the overshoot in electron concentration would occur. The electron concentration at the body is approximately one order of magnitude below the equilibrium normal shock value. Thus the entire shock layer surrounding the nose cap is in a state of extreme nonequilibrium, at temperatures much higher

than equilibrium values. None of the chemical species have reached their equilibrium values at the point where the model surface is reached. The molecular oxygen concentration, for example, is some three orders of magnitude greater than the equilibrium normal shock solution in the entire gaseous envelope. From these computations, the importance of obtaining realistic flow solutions, both in the expansion nozzle and around a model, is apparent for any gaseous radiation experiments.

It is interesting to note the effect of nonequilibrium species in front of the shock on the electron formation behind it. Normal shock solutions were carried out for the test section conditions, and these results are shown in Figure 23. Curve A indicates the electron concentration behind a normal shock in the actual finite rate nozzle test section (i.e. with O, N, NO, O_2, N_2, Ar in front of shock), Curve C_1 has the same initial conditions as Curve A, with the exception that e^- were included in the finite rate expansion. In front of the shock, a frozen concentration of 6×10^9 electrons/cc was computed. It is seen that the electrons start at the ambient value, and asymptotically approach Curve A as the distance behind the shock increases. The initial conditions for Curve C consisted of the same flow velocity, temperature and pressure as the preceding curves, but only the original air composition was assumed (i.e. O_2, N_2, Ar). In this way, only the effect of ambient nonequilibrium species on electron formation could be determined. The production of electrons is delayed considerably, the concentration being some two orders of magnitude lower at corresponding distances behind the shock, for this case as compared with Curve A. Since electrons are formed through the reaction requiring the recombination of an oxygen atom with a nitrogen atom, the availability of these species

immediately behind the shock enables the electrons to be formed at a much faster rate (Curve A).

C. SUMMARY - ANALYSIS PHASE

The finite-rate, normal-shock program for a multicomponent gas has been completed for the IBM-704 computer, and has proven to be an extremely helpful tool in the evaluation of relaxation zones behind the shock waves. A great variety of cases have been run to determine the effects of rate constants, shock velocity, density, etc. on the species formation. This program will continue to be used as a starting point for the more complex bow shock solution.

The general blunt-body problem (i. e. the inviscid, nonequilibrium flow over a blunt axisymmetric body) has been programmed, and subject to final refinements, will be completed in the near future. A number of test cases have been discussed, showing the workability of the program for both re-entry and hypersonic-tunnel test configurations. A higher order fit for the x derivatives is being incorporated into the program to eliminate inaccuracies in the computed body shapes. In addition, more efficient numerical techniques are being incorporated in the program in order to decrease the computing time.

APPENDIX -- DETERMINATION OF THE EFFECTS OF INTERNAL REFLECTION IN THE SHOCK TUBE

The low emissivities of the radiating gases making them optically thin, requires that the effect of reflections inside the shock tube be taken into account. The shock tube is Kanigen plated internally and this chemically-deposited nickel-phosphorous plating renders the tube very shiny to the eye, and suggests a reflection coefficient greater than .5 .

It has been mentioned in the report that the effective aperture into the shock tube is a rectangular 1 x 12 mm image of the detector on the shock tube window. Because the inside of the window is contoured to the 3-inch inside diameter of the tube, it behaves like a cylindrical lens. Figure 9 is a sketch of the cross section of the shock tube at the window, showing the accepted field of view. Opposite this window is another window port, which, for these studies, was plugged with a window which was "potted" into its frame with an epoxy resin doped with carbon black. Thus, the reflection coefficient of this part of the wall was decreased to that of the air-sapphire interface. It was measured to be 0.05. It should be mentioned that for reasons of spectroscopic cleanliness no simple coating of paint, plastic, tape, etc., could be tolerated in an effort to decrease the wall reflectance. From the figure it can be seen that the wall of the shock tube opposite the window is now a composite of plated metal and the sapphire window.

Shock tube runs were made such that the conditions of the gas within the tube were identical. In one case the full viewing optics were used (1 x 12 mm slit) and in the second the slit was masked to 1 x 1 mm. With an aperture of this size,

the solid angle subtended by the spectrometer was such as to limit the field of view on the other side of the tube to an area completely bounded by the sapphire window. This is also shown in Figure 9. For these experiments, which were performed at .9 microns, a Dumont K-1430 infrared-sensitive photomultiplier was used to obtain a better signal-to-noise ratio than could be obtained with the PbSe cells.

Because the radiation from the gas was the same in the experiments, the ratio of the two recorded intensities were directly related to the averaged reflections within the shock tube. The effects of varying angles of incidence inside the tube, as well as multiple reflections are thus automatically compensated. This average value of the reflection coefficient from the walls was measured to be 0.4 ± 0.05.

REFERENCES

1. Wurster, W. H. and Marrone, P. V., Study of Infrared Emission in Heated Air, Semi-Annual Report, December 1960, CAL Report No. QM-1373-A-3.

2. Wurster, W. H. and Marrone, P. V., Study of Infrared Emission in Heated Air, Semi-Annual Report, December 1959, CAL Report. No. QM-1373-A-1.

3. Wurster, W. H. and Marrone, P. V., Study of Infrared Emission in Heated Air, Annual Report, May 1960, CAL Report No. QM-1373-A-2.

4. Stewart, D. T., Journal of Atmospheric and Terrestrial Physics, Vol. 10, 318, 1957.

5. Kaufman, F., Proc. Roy. Soc. A, Vol. 247, 123, 1958.

6. Garvin, D., Gwyn, P., and Moskowitz, J., Canadian Journ. Chem, Vol. 38, 153, 1960.

7. Fontijn, A. and Schiff, H. I., Absolute Rate Constant for Light Emission of the Air Afterglow Reaction for the Wavelength Region 3875-6200A. Advance Papers of the International Symposium on Chemical Reactions in the Lower and Upper Atmosphere, (SRI), San Francisco, California, April 1961.

8. Treanor, C. E. and Wurster, W. H., Measured Transition Probabilities for the Schumann-Runge System of Oxygen, AFOSR TN-59-964, J. Chem. Phys. 32, 758, 1960.

9. Keck, J., Camm, J., Kivel, B., and Wentink, T., Annals of Physics 7, 1, 1959.

10. Harteck, P., Reeves, R. and Mannella, G., J. Chem. Phys. 29, 1333, December 1958.

11. Logan, J. G. Jr. and Treanor, C. E., Tables of Thermodynamic Properties of Air from 3000°K to 10,000°K, CAL Report No. BE-1007-A-3, 1957.

12. Wurster, W. H. and Treanor, C. E., Spectroscopic Technique for Temperature-Density Measurements in Oxygen-Bearing Flows, CAL Report No. AD-1118-A-10, December 1959 (AFOSR TN-59-1089).

13. Wurster, W. H., High-Speed Shutter for Spectrographs, Rev. Sci. Inst. 28, 1093, 1957.

14. Gilmore, F. R., Equilibrium Composition and Thermodynamic Properties of Air to 24,000°K, Rand Research Memorandum RM-1543, 1955.

15. Broida, H. P., Schiff, H. I., and Sugden, T. M., Observations on the Chemiluminescent Reaction of Nitric Oxide with Atomic Oxygen, Trans. Faraday Soc., 57, 259, 1961.

16. Stair, R., Johnston, R. G., and Halbach, E. W., Journ. Res. NBS, Vol. 64A, No. 4, July-August 1960.

17. Dieke, G. H. and Heath, D. F., The First and Second Positive Bands of N_2, Johns Hopkins Spectrographic Report No. 17, December 1959.

18. Jarmain, W. R. and Nicholls, R. W., Vibrational Transition Probabilities to High Quantum Numbers for the Nitrogen First and Second Positive Band Systems. Can. Journ. Phys., Vol. 32, 201, 1954.

19. Taylor, R. L., Continuum Infrared Spectrum of High Temperature Air, AVCO Research Report No. 88, June 1960.

20. Cheng, H. K., Hypersonic Shock Layer Theory of the Stagnat: Region at Low Reynolds Number. Cornell Aeronautical Laboratory Report No. AF-1285-A-7, April 1961. Presented at the 1961 Heat Transfer and Fluid Mechanics Institute, University of Southern California, Los Angeles.

21. Scala, Sinclair M., Hypersonic Viscous Shock Layer, American Rocket Society Journal, July 1959, p. 520.

22. Duff, Russell E. and Davidson, Norman, Calculation of Reaction Profiles Behind Steady State Shock Waves, II. The Dissociation of Air, The Journ. Chem. Phys. Vol. 31, No. 4, October 1959.

23. Teare, J. D. and Dreiss, G. J., Theory of the Shock Front, III. Sensitivity to Rate Constants. AVCO Research Note 176, December 1959.

24. Lick, W., Inviscid Flow Around a Blunt Body of a Reacting Mixture of Gases. Part A, General Analysis, Rensselaer Polytechnic Institute TRAE 5810 (AFOSR TN-58-522), May 1958. Part B, Numerical Solutions RPI TRAE 5814 (AFOSR TN-58-2114), December 1958.

25. Li, Ting-Yi and Geiger, Richard E., Stagnation Point of a Blunt Body in Hypersonic Flow, Jour. Aero. Sciences, p. 25, January 1957.

26. Eschenroeder, A. Q., Boyer, D. W., and Hall, J. G., Exact Solutions for Nonequilibrium Expansions of Air with Coupled Chemical Reactions. CAL Report No. AF-1413-A-1, May 1961.

ACKNOWLEDGEMENT

The authors wish to acknowledge the helpful discussions and the contributions by Drs. C. E. Treanor and A. Q. Eschenroeder, and the assistance of Mr. L. Garr in the IBM 704 programming and Mr. H. Thompson in the radiation experiments. The numerical results pertaining to the hypersonic tunnel configuration were taken from computations performed for the Air Research and Development Command, Rome Air Development Center, Griffiss Air Force Base, New York, under Contract No. AF 30(602)-2267.

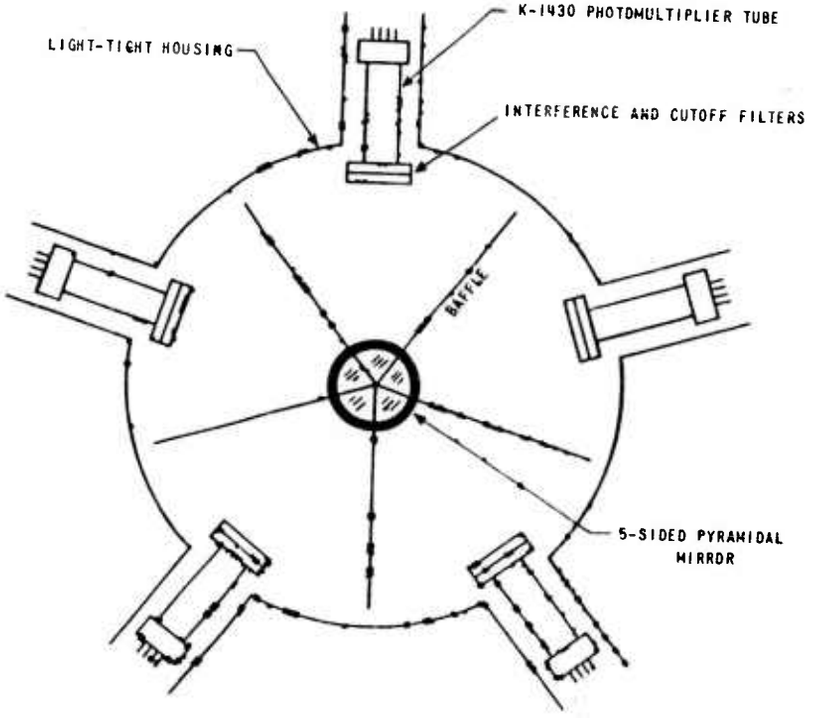

Figure 1 A SCHEMATIC VIEW OF THE 5 CHANNEL PHOTOMULTIPLIER-FILTER ASSEMBLY. INCIDENT RADIATION (NORMAL TO THE PLANE OF THE PAPER) IS DEFLECTED BY THE MIRROR ASSEMBLY INTO THE RESPECTIVE WAVELENGTH CHANNELS.

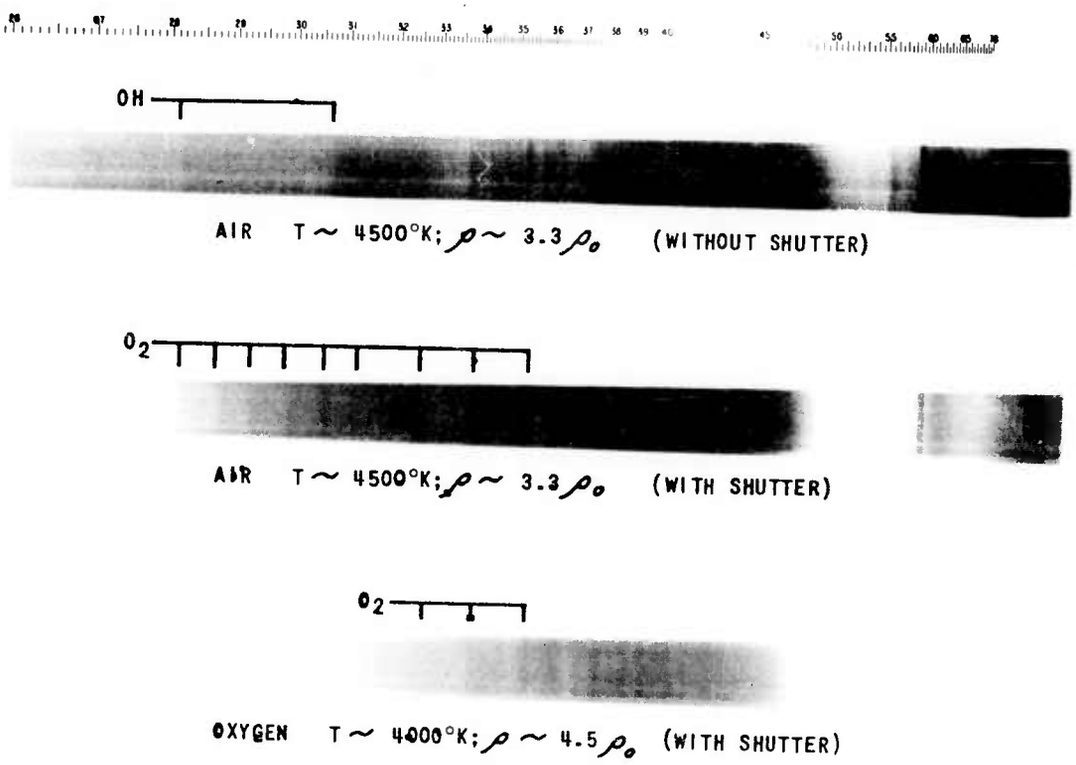

Figure 2 SHOCK TUBE SPECTRA

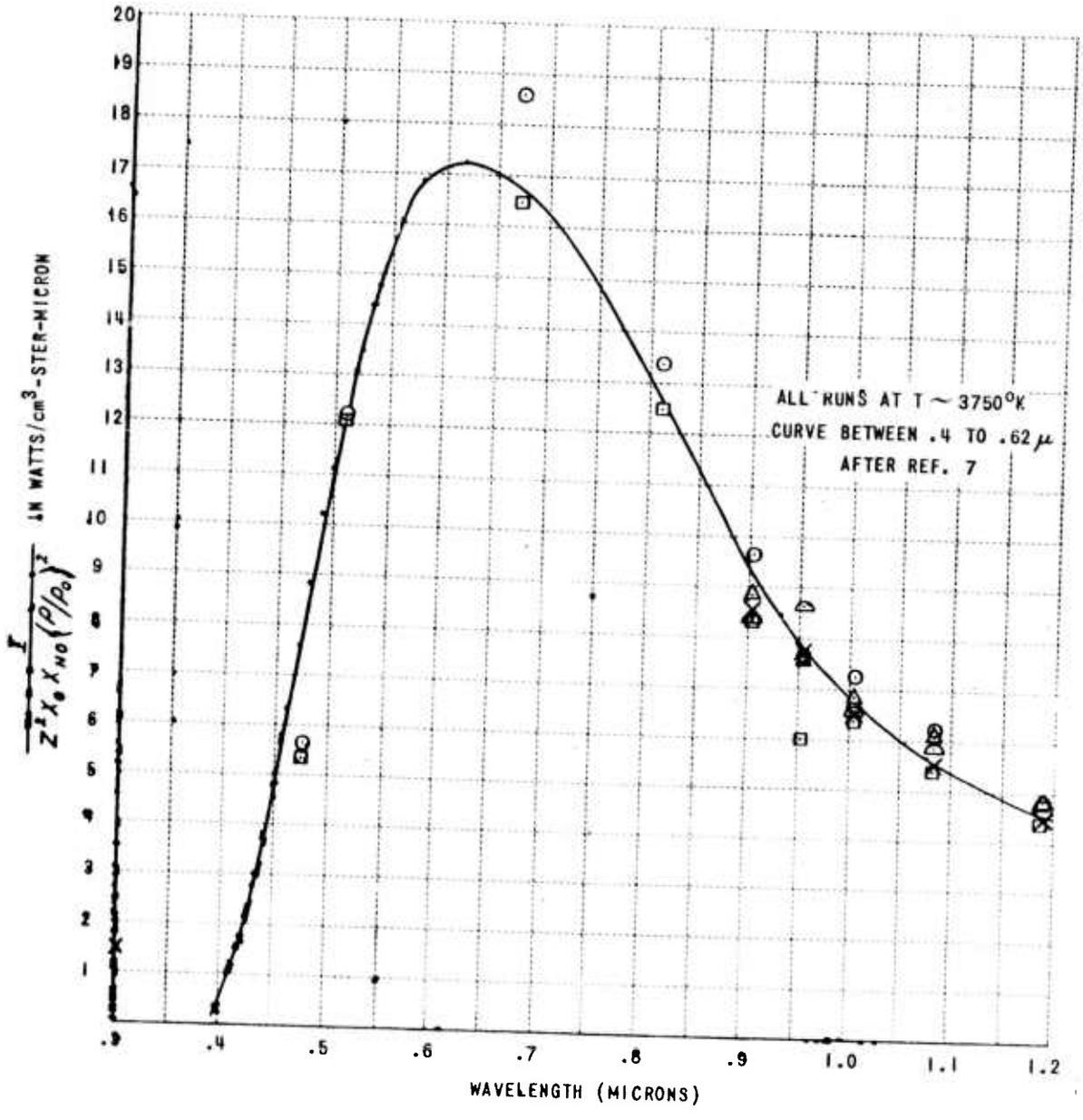

Figure 3 THE NO-Q CONTINUUM SPECTRUM

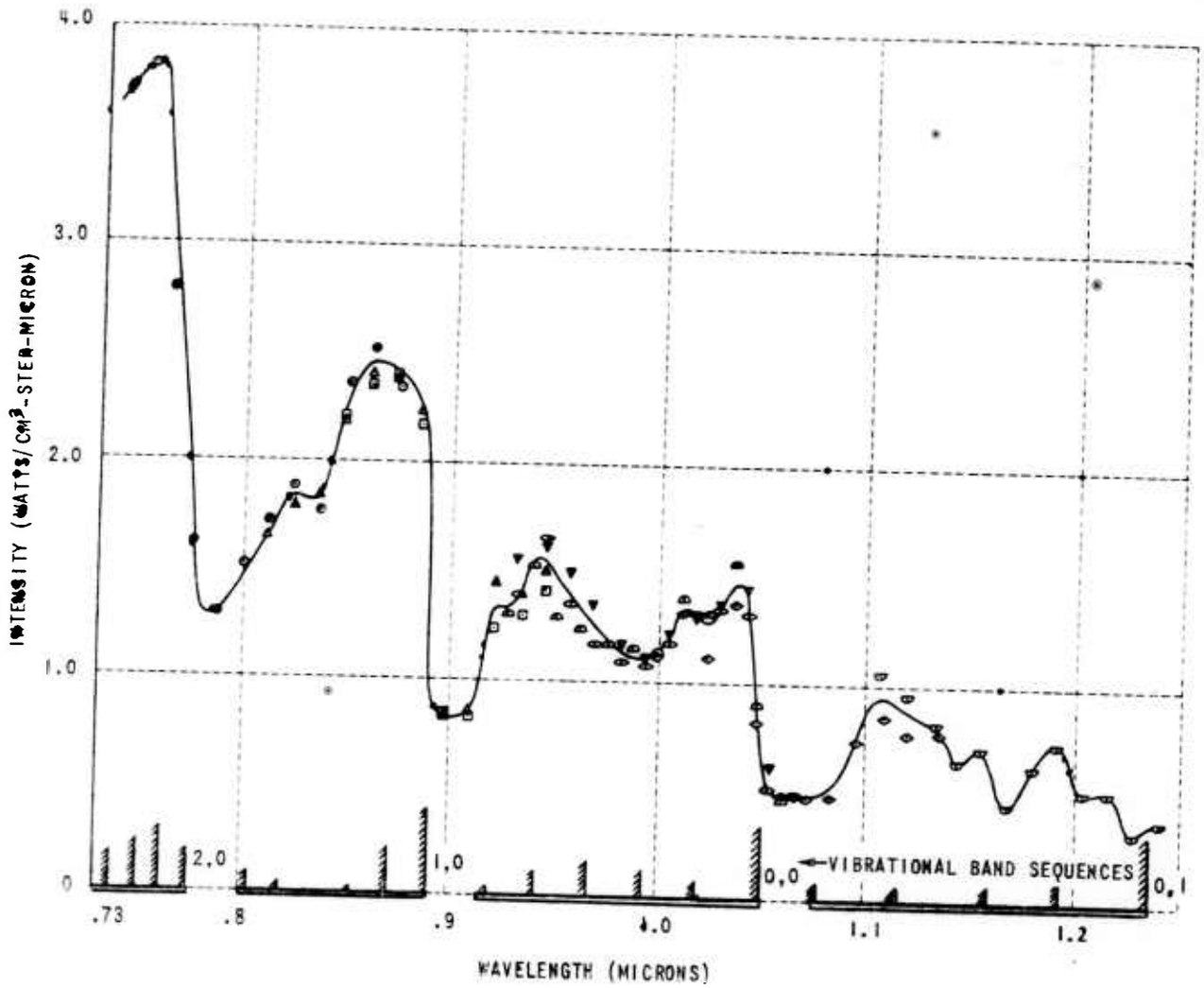

Figure 4 INFRARED SPECTRAL INTENSITY IN THE FIRST POSITIVE BAND SYSTEM OF NITROGEN

$T = 5630°K$; $\rho = .88\,\rho_0$

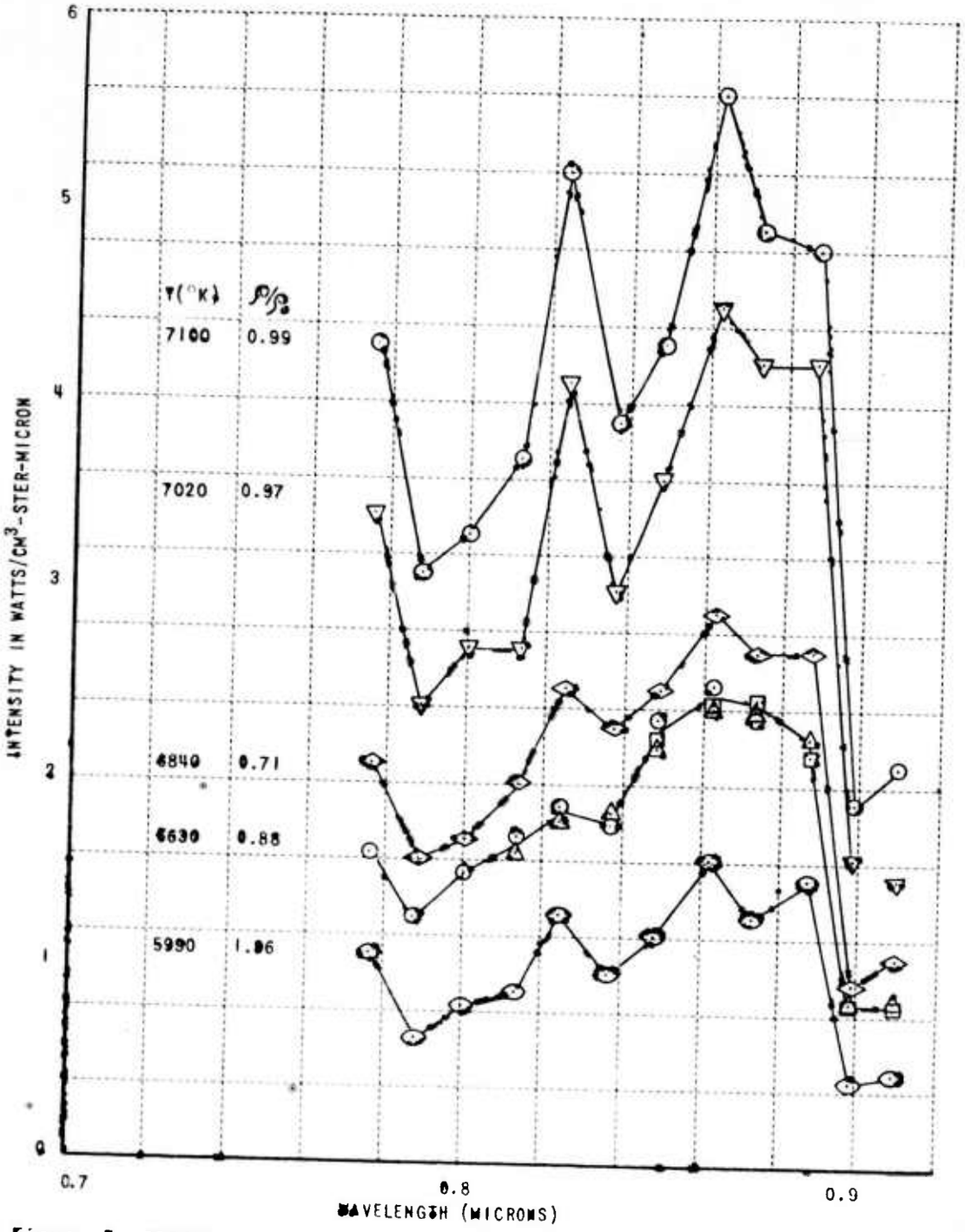

Figure 5 SPECTRA OF THE $v'=1$, $v''=0$ SEQUENCE OF THE FIRST POSITIVE SYSTEM OF NITROGEN

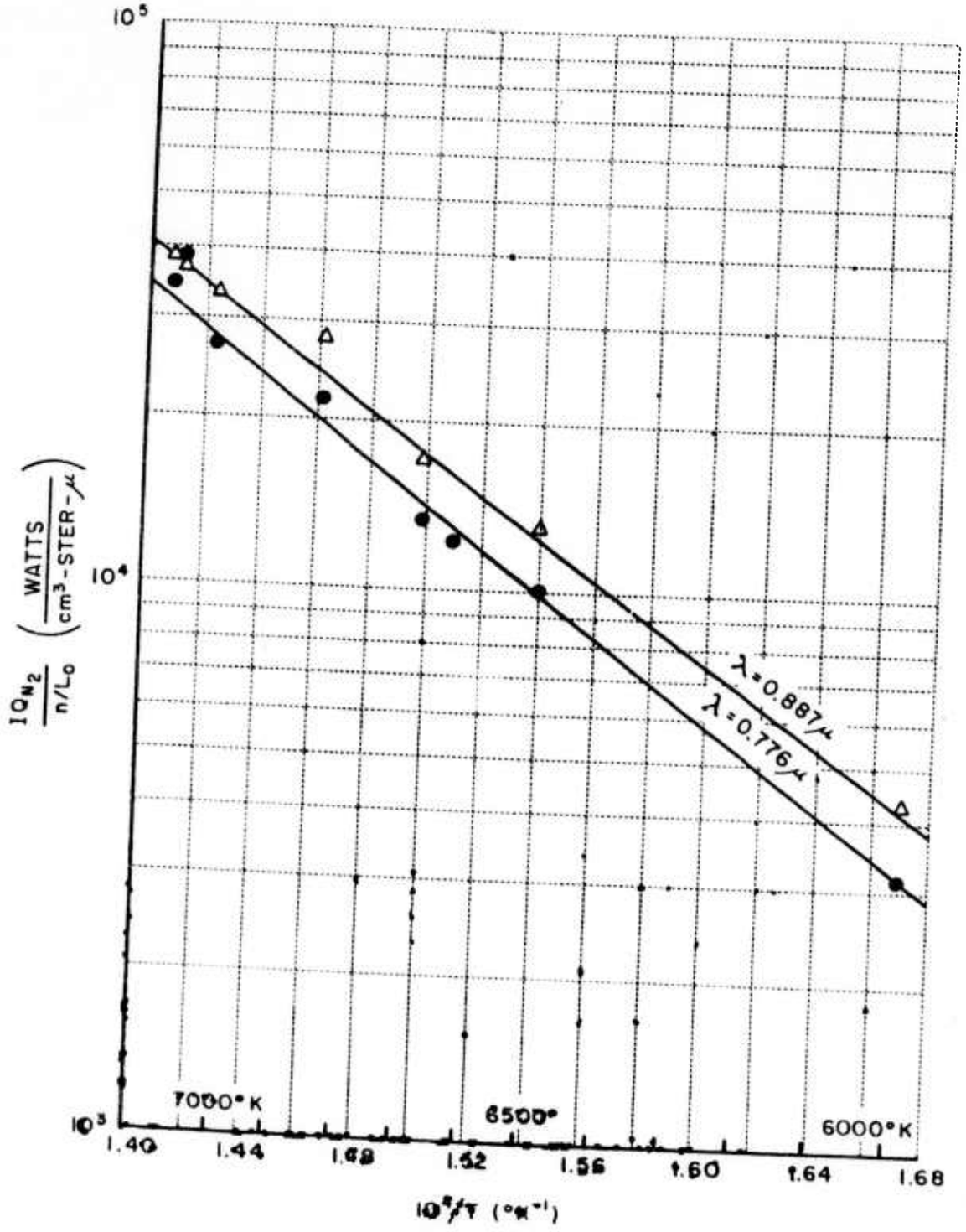

Figure 6 TEMPERATURE DEPENDENCE OF THE MEASURED INTENSITY OF THE NITROGEN SPECTRUM

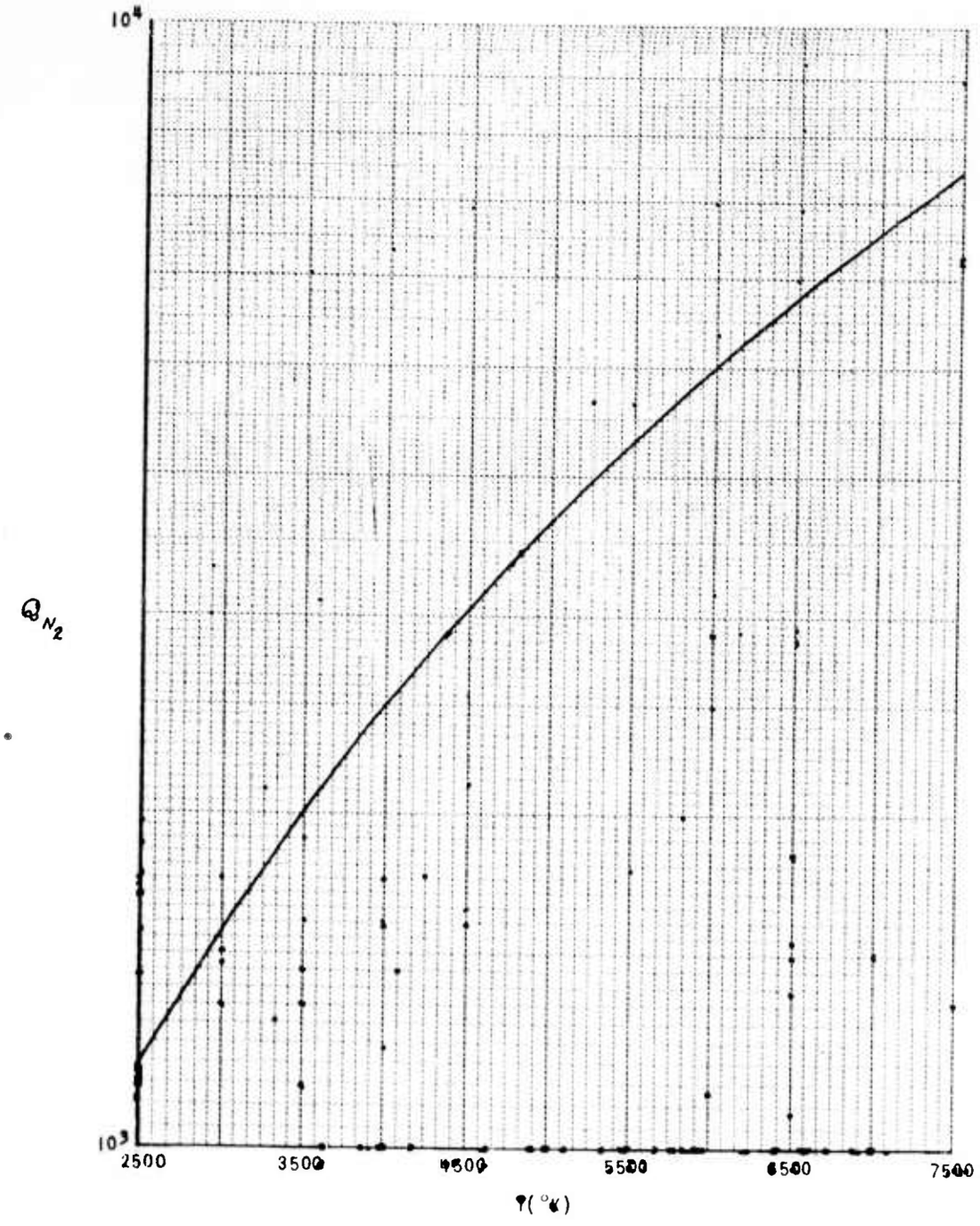

Figure 7 INTERNAL PARTITION FUNCTION FOR NITROGEN (REF. 63)

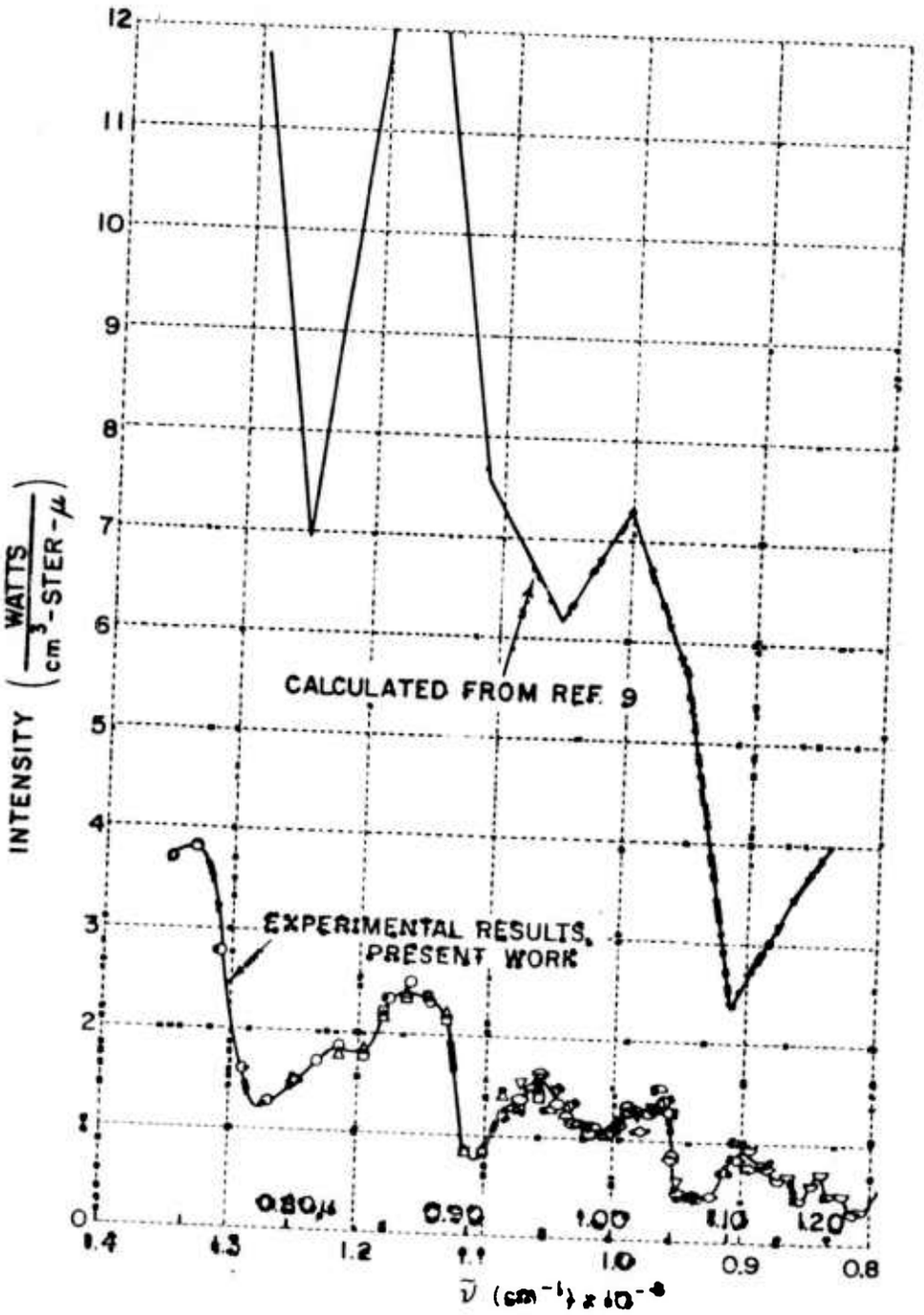

Figure 8 RADIATION FROM NITROGEN (1+)
T = 6630°K, $\rho = 0.88\rho_0$

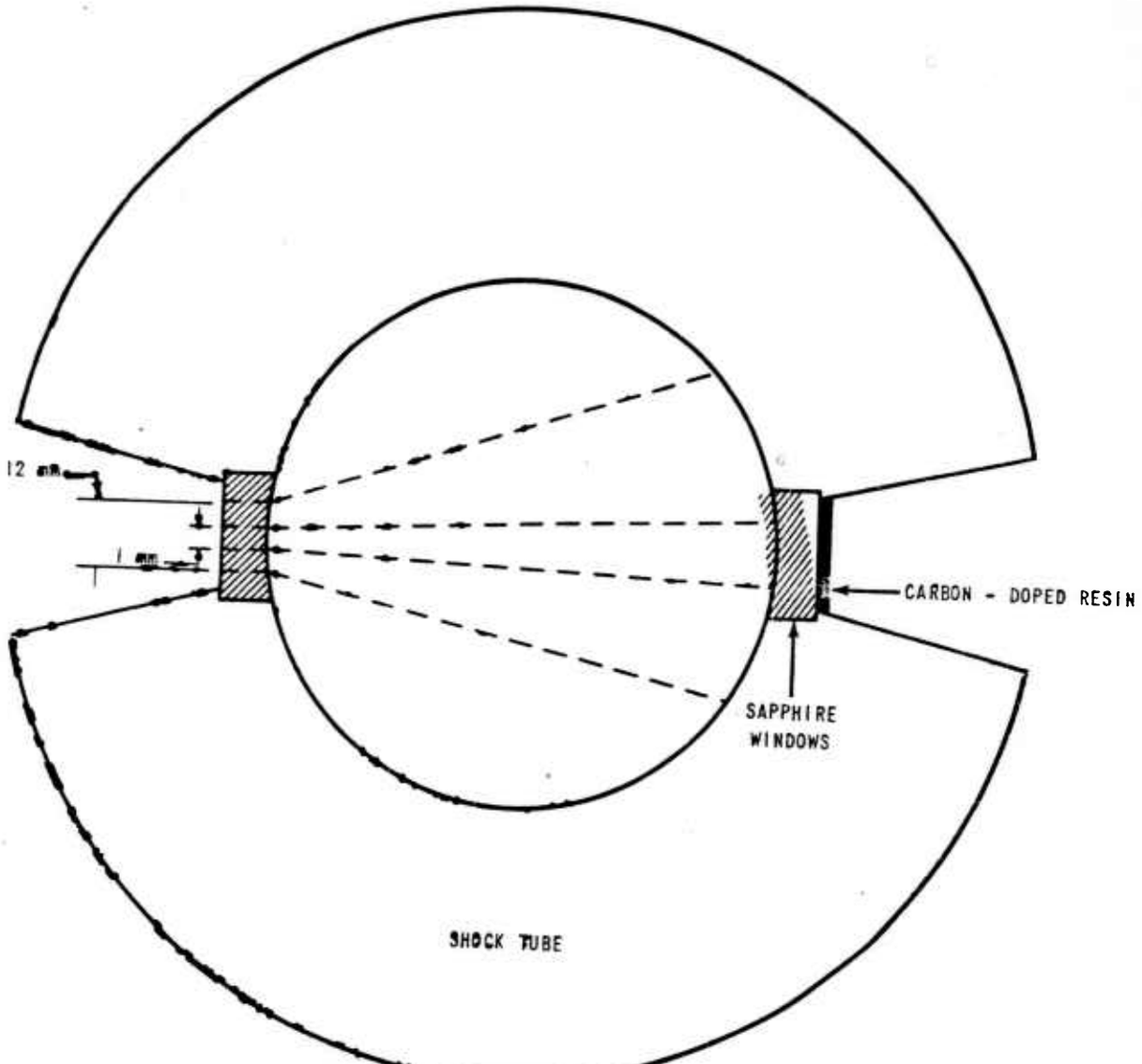

Figure 9 OPTICAL GEOMETRY INSIDE THE SHOCK TUBE FOR THE REFLECTION COEFFICIENT MEASUREMENTS. (SEE APPENDIX FOR DETAILS)

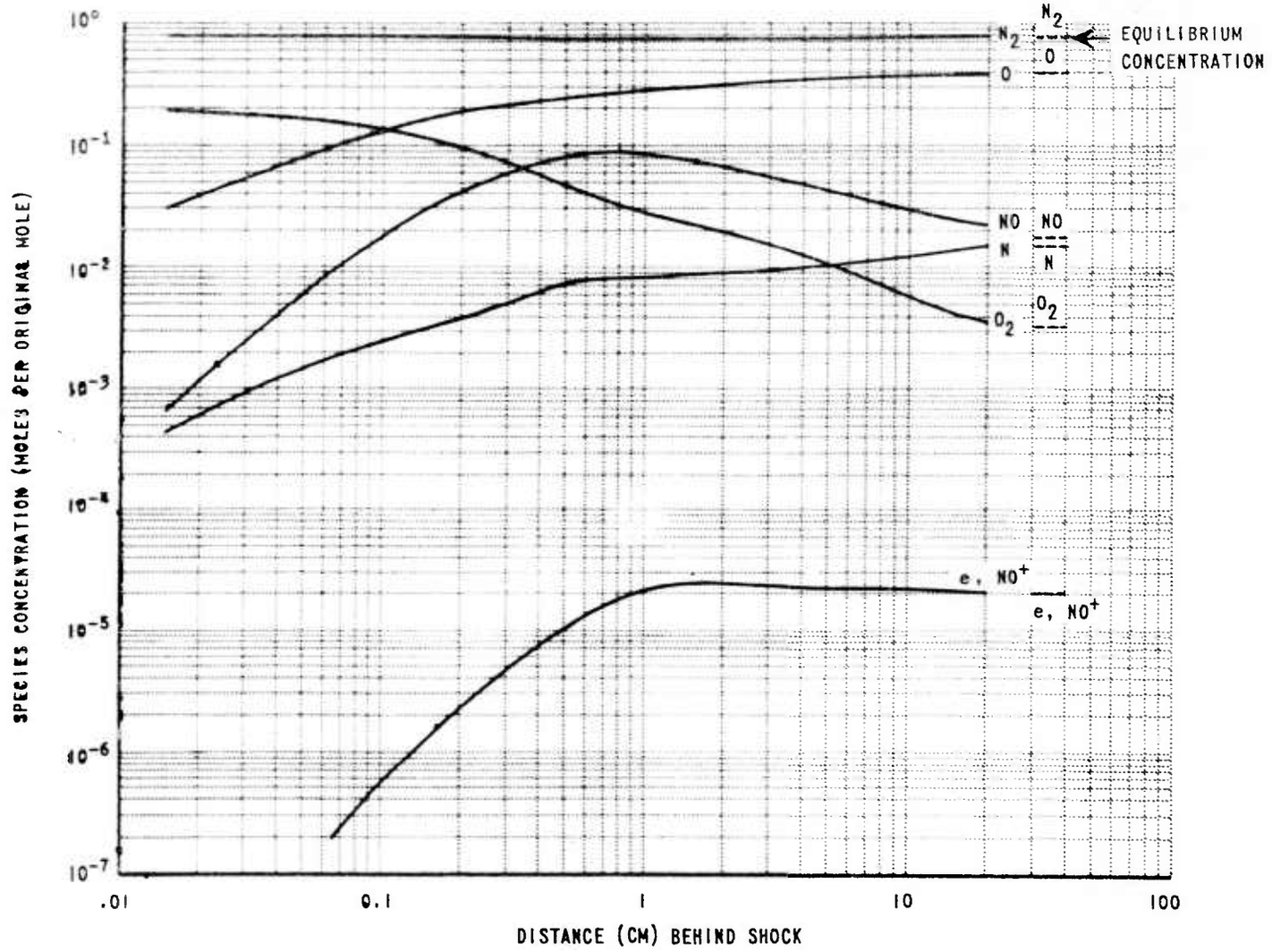

Figure 10 SPECIES CONCENTRATION BEHIND NORMAL SHOCK IN AIR

$M_S = 12.28$ $T_1 = 300\ ^\circ K$ $P_1 = 1.0$ mm Hg

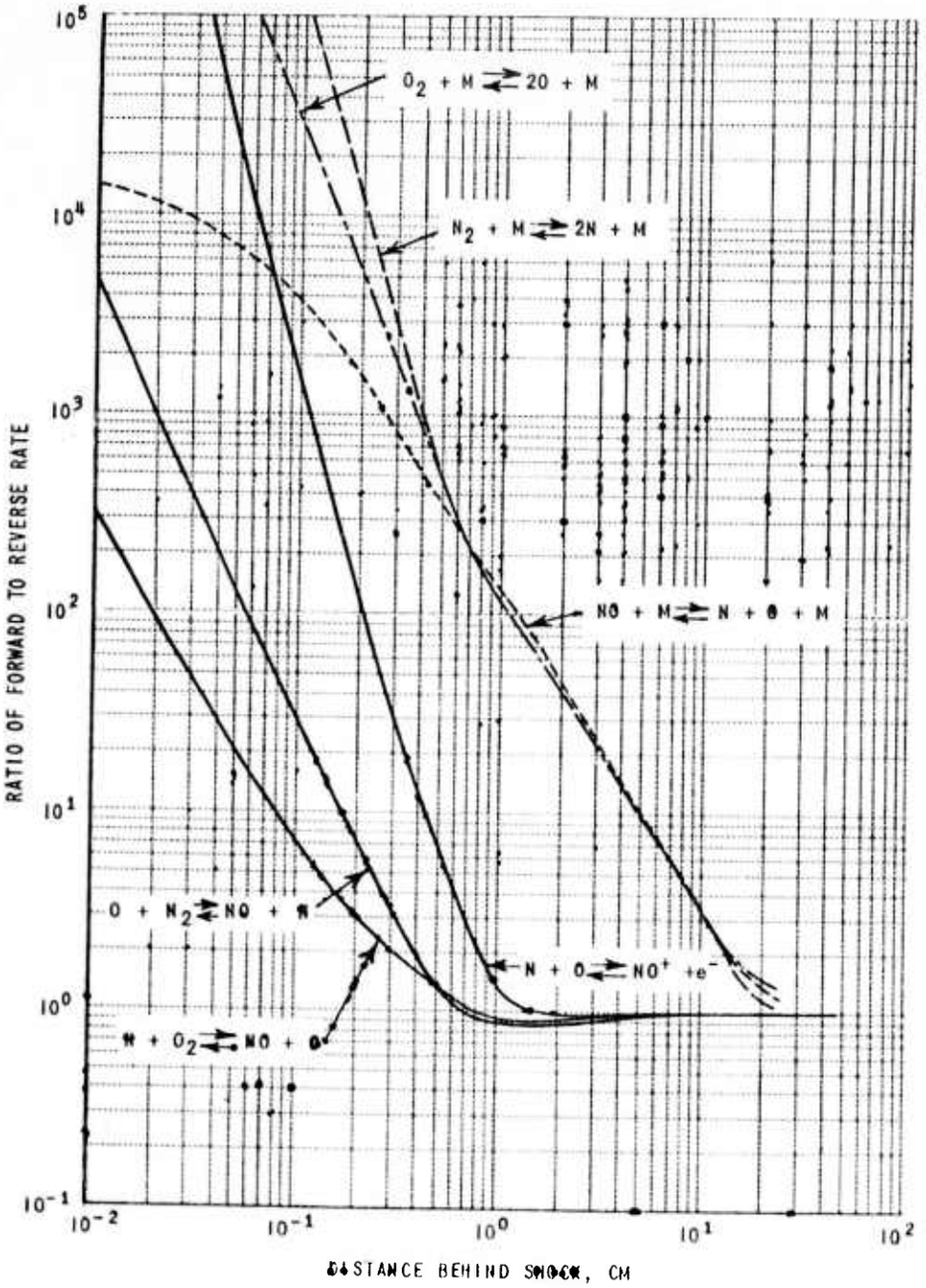

Figure 11 RATIO OF FORWARD TO REVERSE RATES BEHIND NORMAL SHOCK IN AIR

$M_s = 12.3$ $P_1 = 1.0$ mm Hg $T_1 = 300^\circ K$

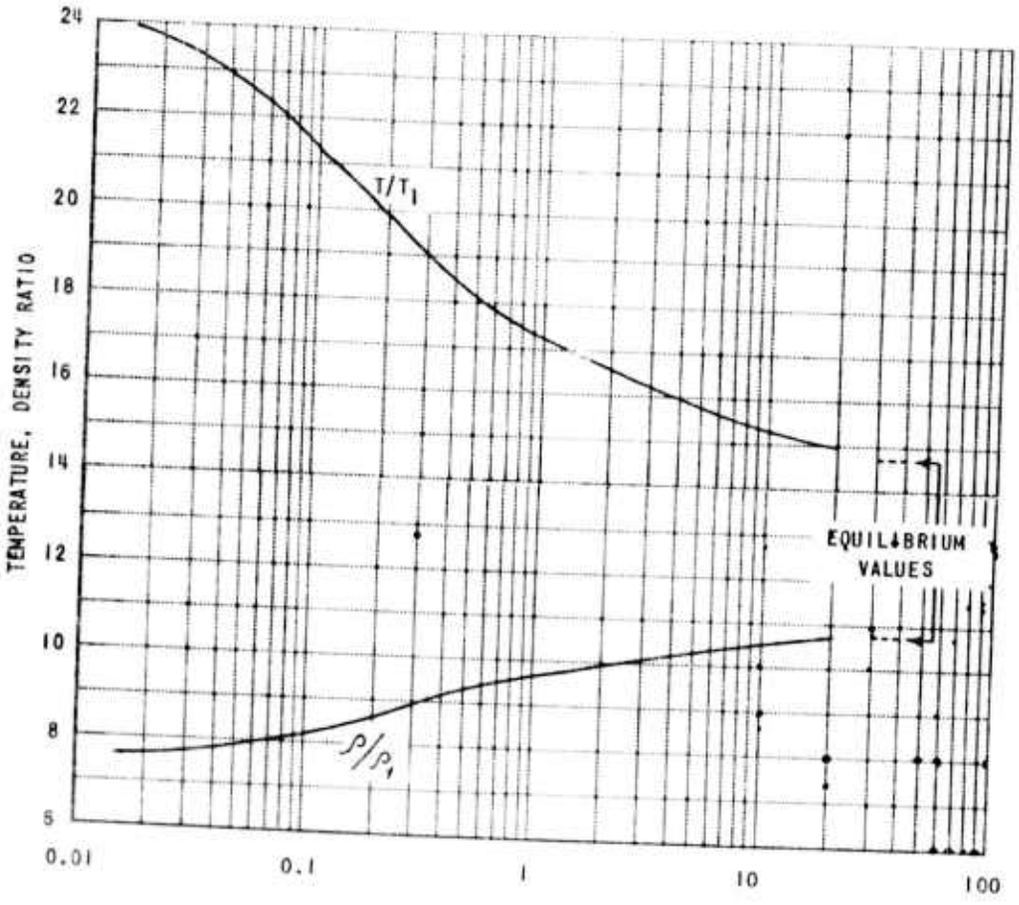

Figure 12 TEMPERATURE AND DENSITY DISTRIBUTION BEHIND NORMAL SHOCK IN AIR

M_s = 12.28 T_1 = 300°K P_1 = 1.0 mm Hg

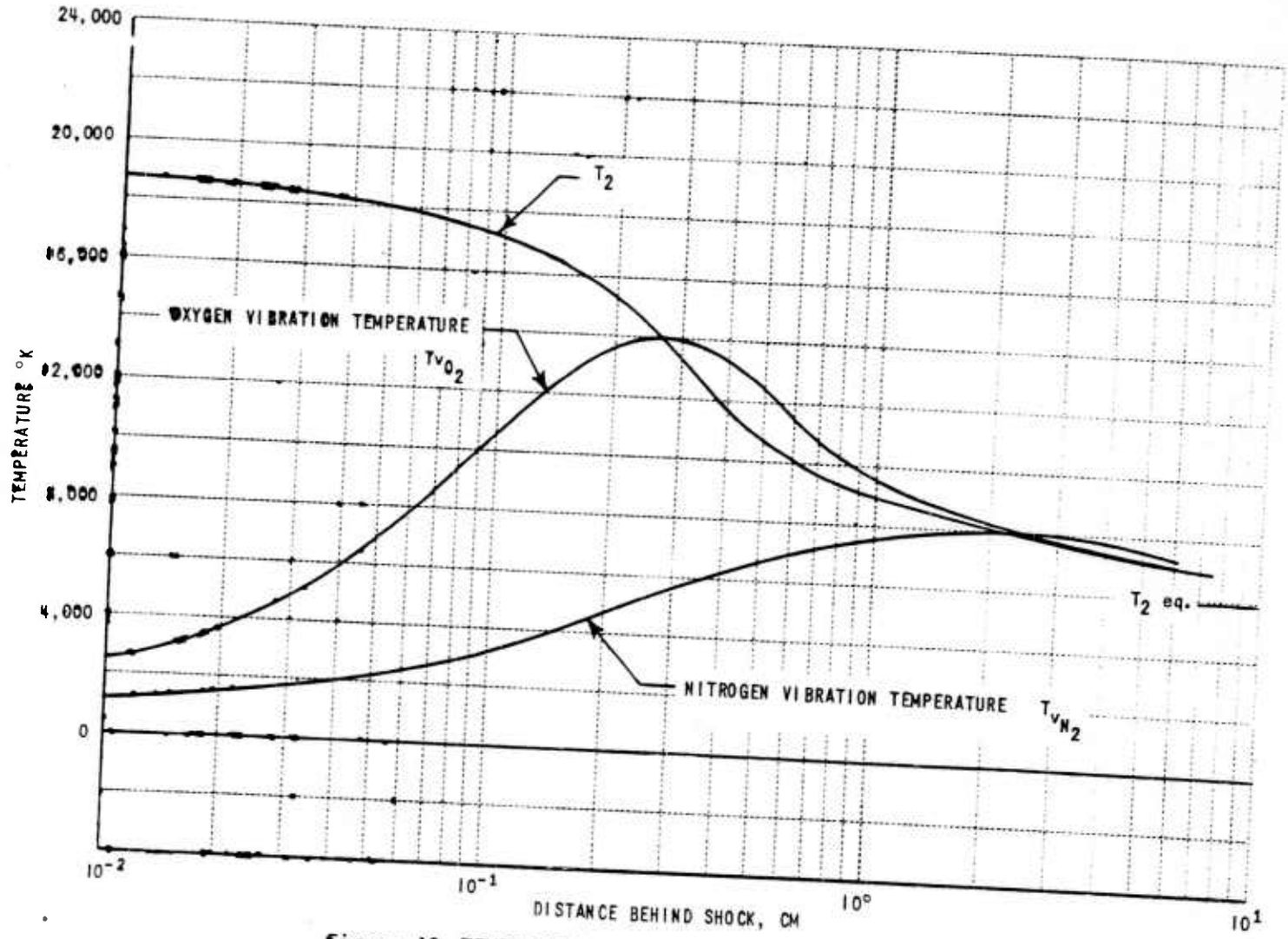

Figure 13 TEMPERATURE BEHIND NORMAL SHOCK WAVE IN AIR

$M_s = 19$ $P_1 = 100\,\mu Hg$ $T_1 = 300°K$

(VIBRATIONAL NONEQUILIBRIUM WITH COUPLING)

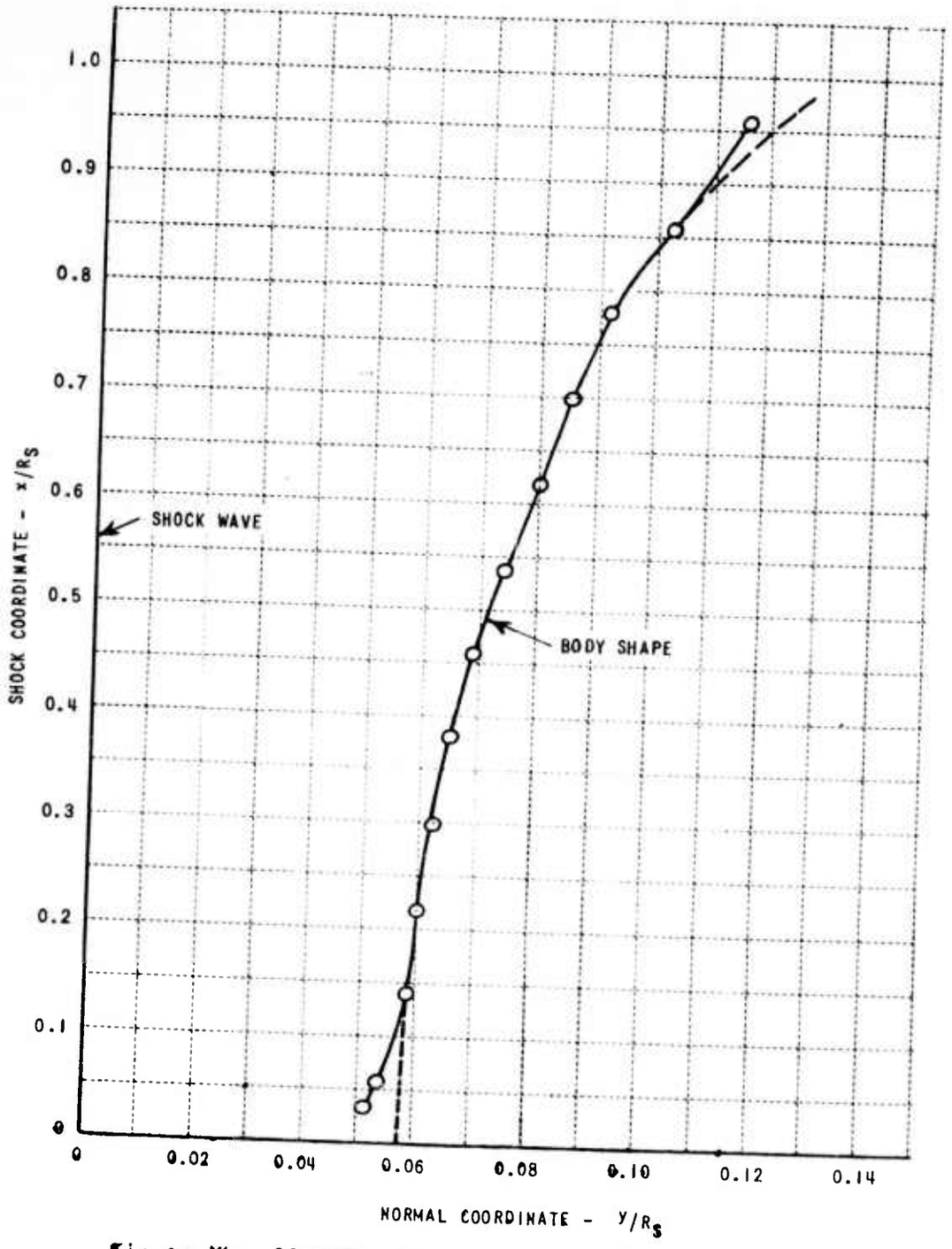

Figure 14a COMPUTED BODY SHAPE IN SHOCK COORDINATE SYSTEM

ALTITUDE = 200,000 ft. VELOCITY = 23,000 ft/sec.
CATENARY SHOCK; 15 CM RADIUS AT CENTERLINE

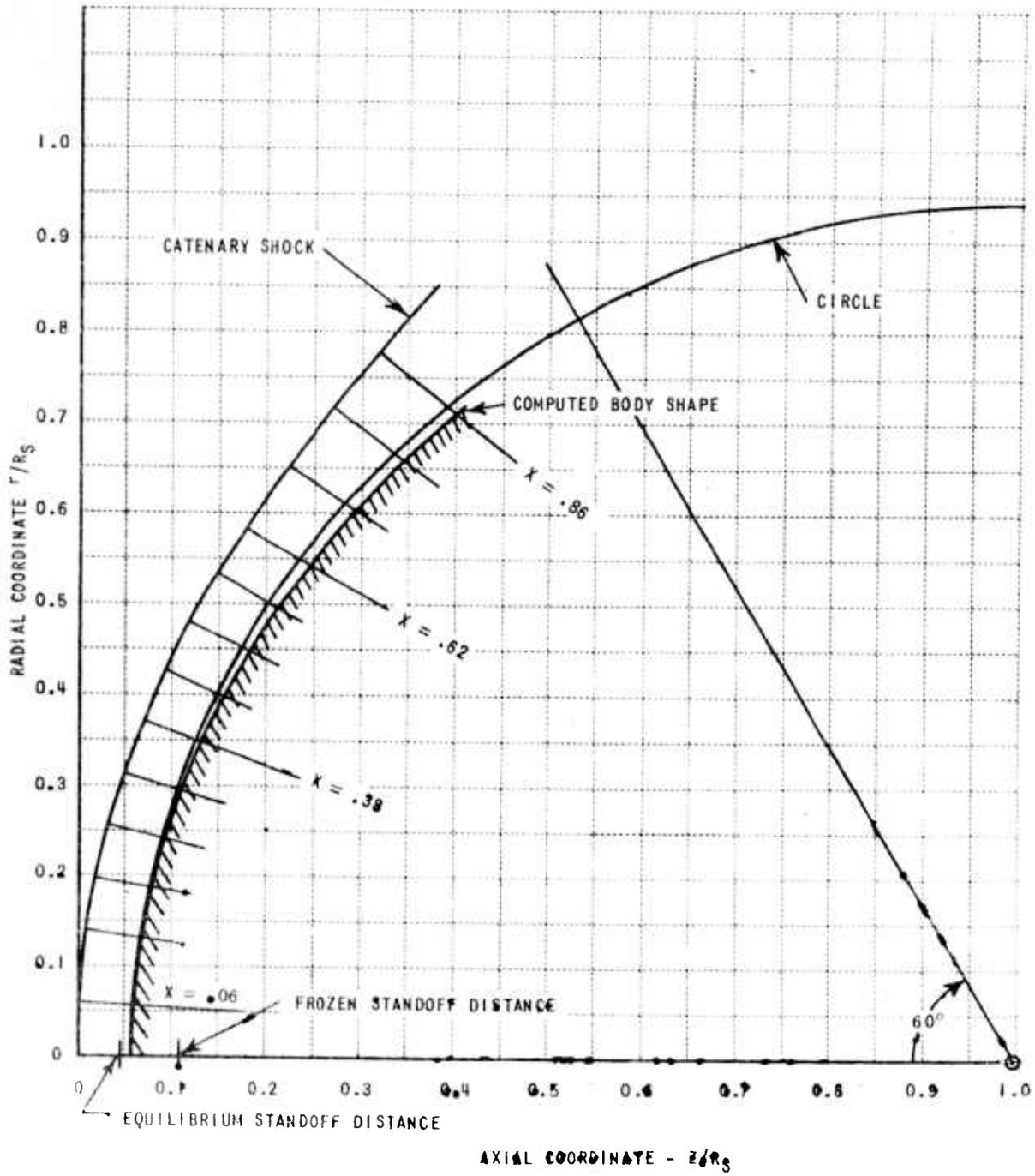

Figure 14b COMPUTED BODY SHAPE IN AXISYMMETRIC COORDINATE SYSTEM

ALTITUDE = 200,000 ft. VELOCITY = 23,000 ft/sec.
CATENARY SHOCK; 15 CM RADIUS AT CENTERLINE

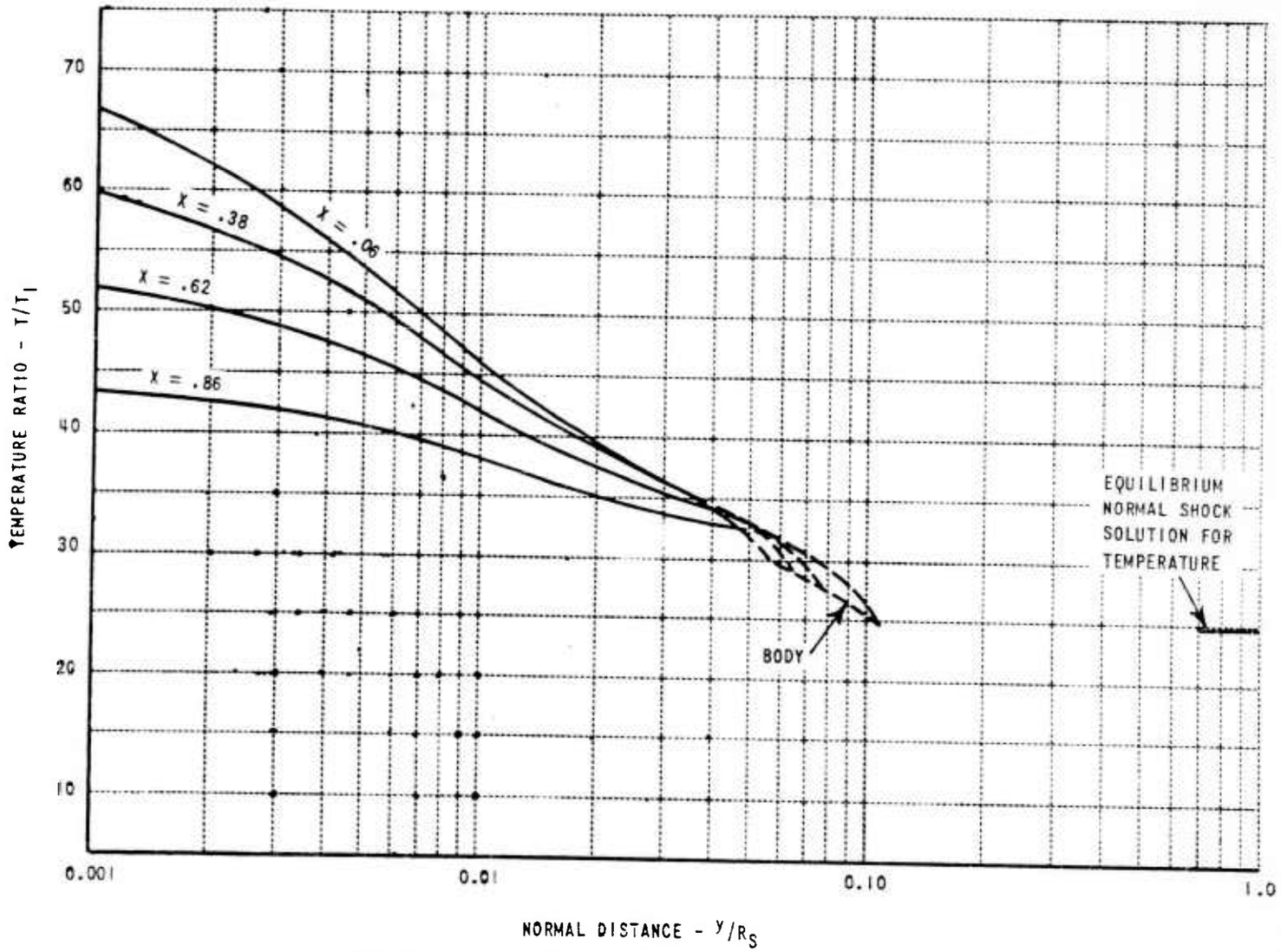

Figure 15 TEMPERATURE DISTRIBUTION AROUND NOSE OF RE-ENTRY VEHICLE

ALTITUDE = 200,000 ft. VELOCITY = 23,000 ft/sec.
CATENARY SHOCK: 15 CM RADIUS AT CENTERLINE $T_1 = 249^{\circ}K$

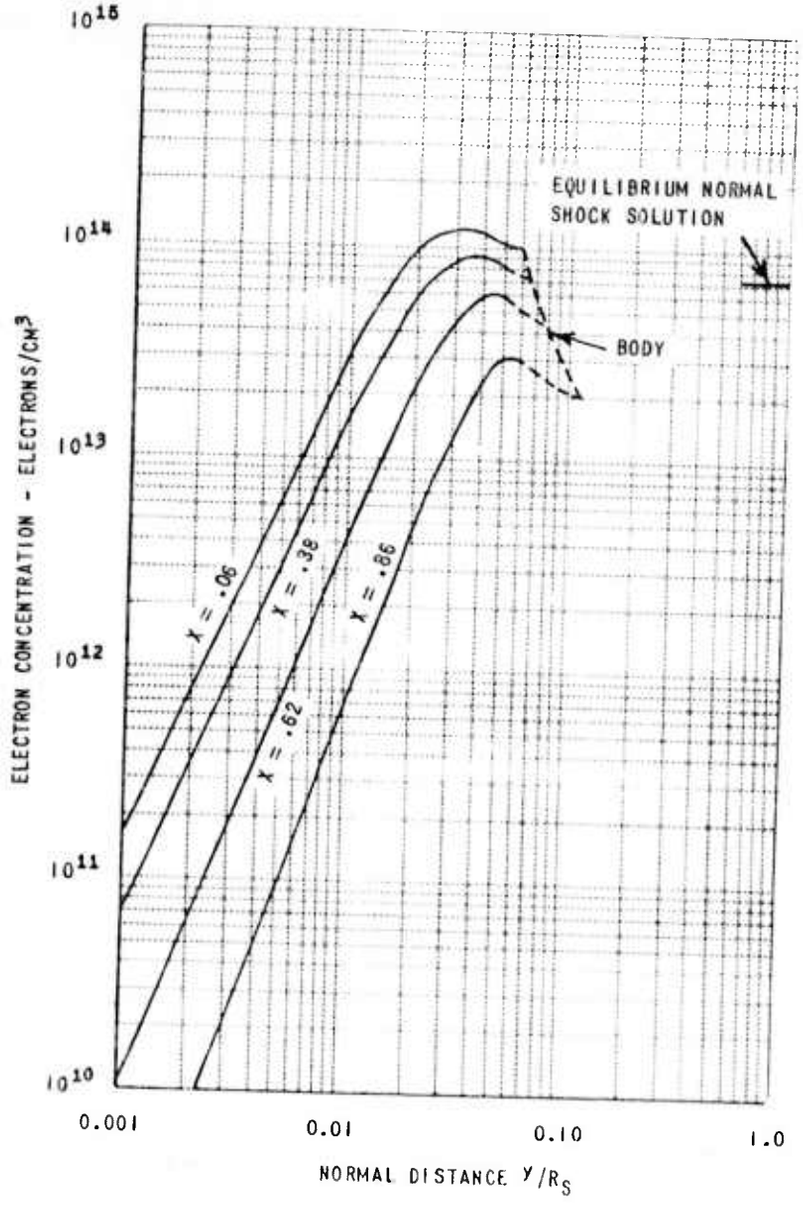

Figure 16 ELECTRON CONCENTRATION AROUND NOSE OF RE-ENTRY VEHICLE

ALTITUDE = 200,000 ft. VELOCITY = 23,000 ft/sec.
CATENAPY SHOCK, 15 CM RADIUS AT CENTERLINE

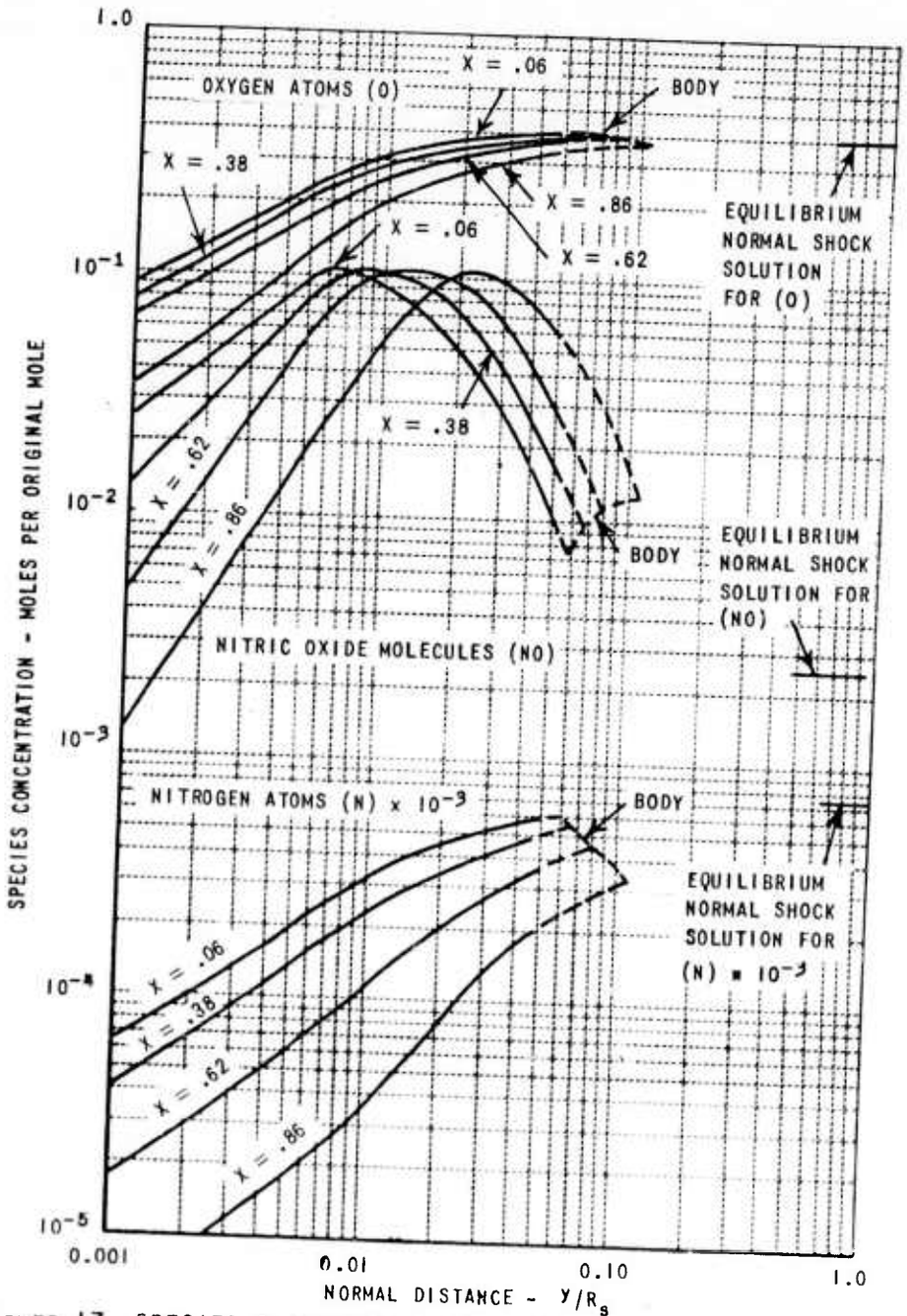

Figure 17 SPECIES CONCENTRATION AROUND NOSE OF RE-ENTRY VEHICLE

ALTITUDE = 200,000 ft. VELOCITY = 23,000 ft/sec
CATENARY SHOCK; 15 CM RADIUS AT CENTERLINE

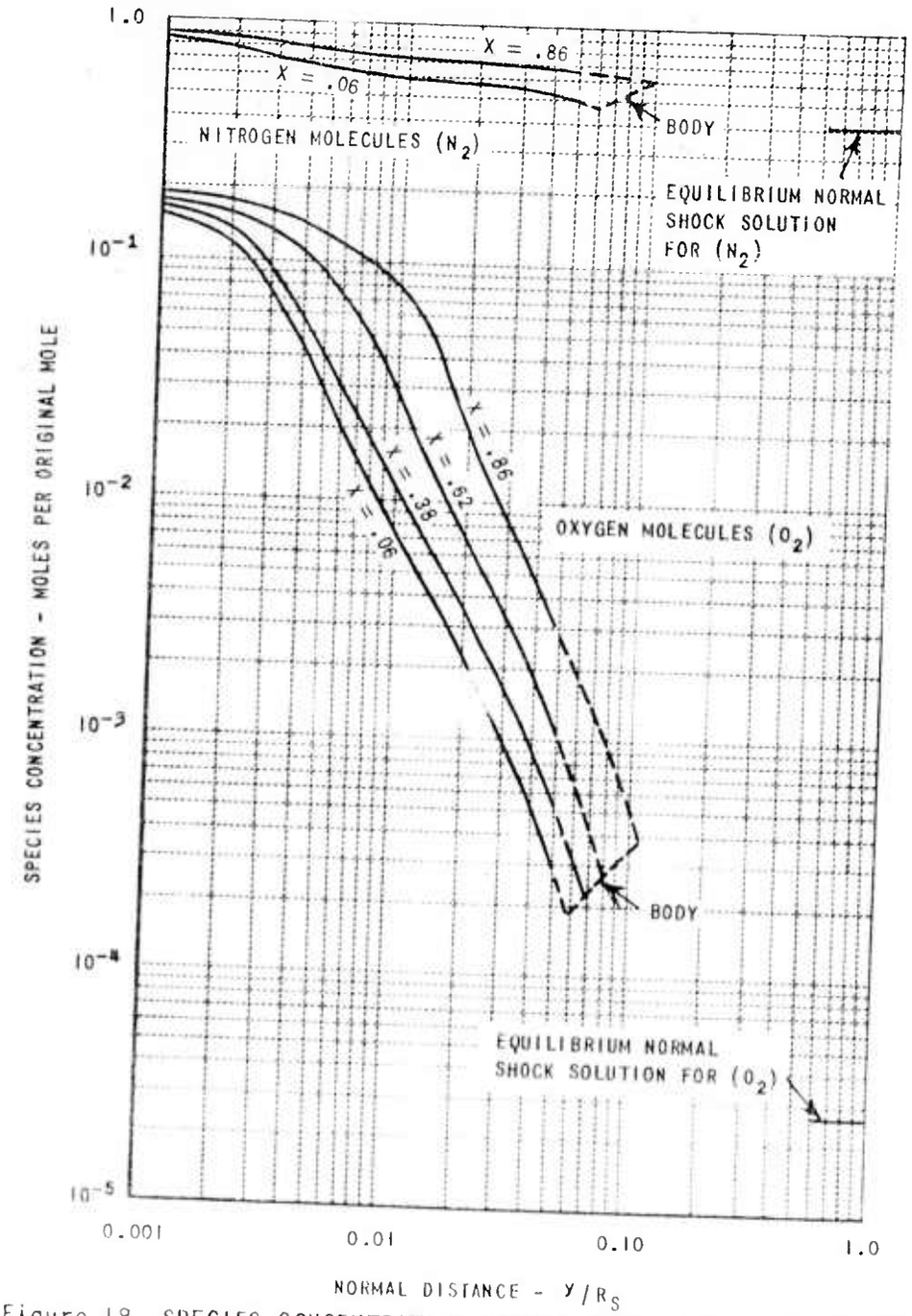

Figure 18 SPECIES CONCENTRATION AROUND NOSE OF RE-ENTRY VEHICLE

ALTITUDE = 200,000 ft. VELOCITY = 23,000 ft/sec.
CATENARY SHOCK; 15 CM RADIUS AT CENTERLINE

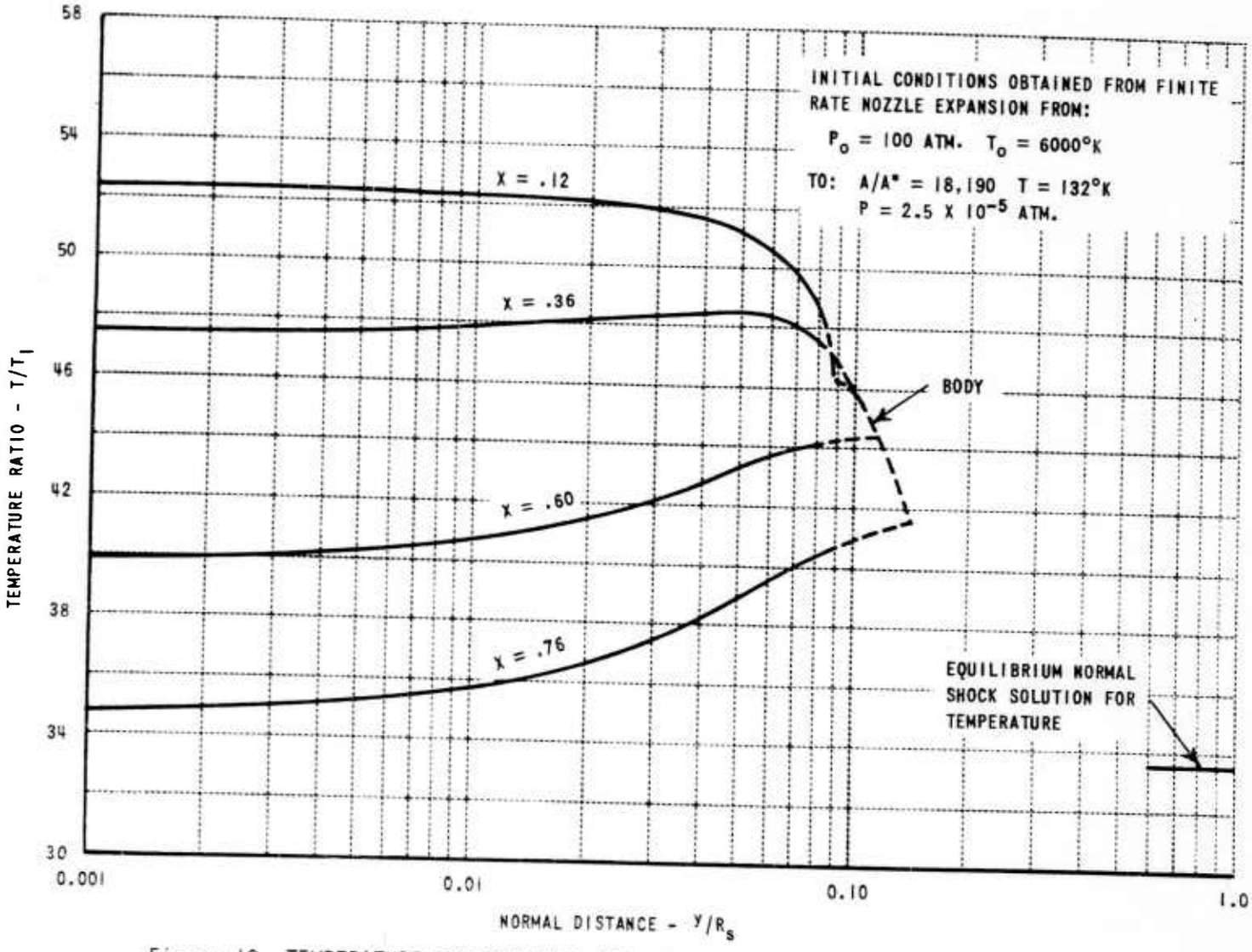

Figure 19 TEMPERATURE DISTRIBUTION AROUND NOSE OF HYPERSONIC VEHICLE

CATENARY SHOCK: 16.15 CM RADIUS AT CENTERLINE

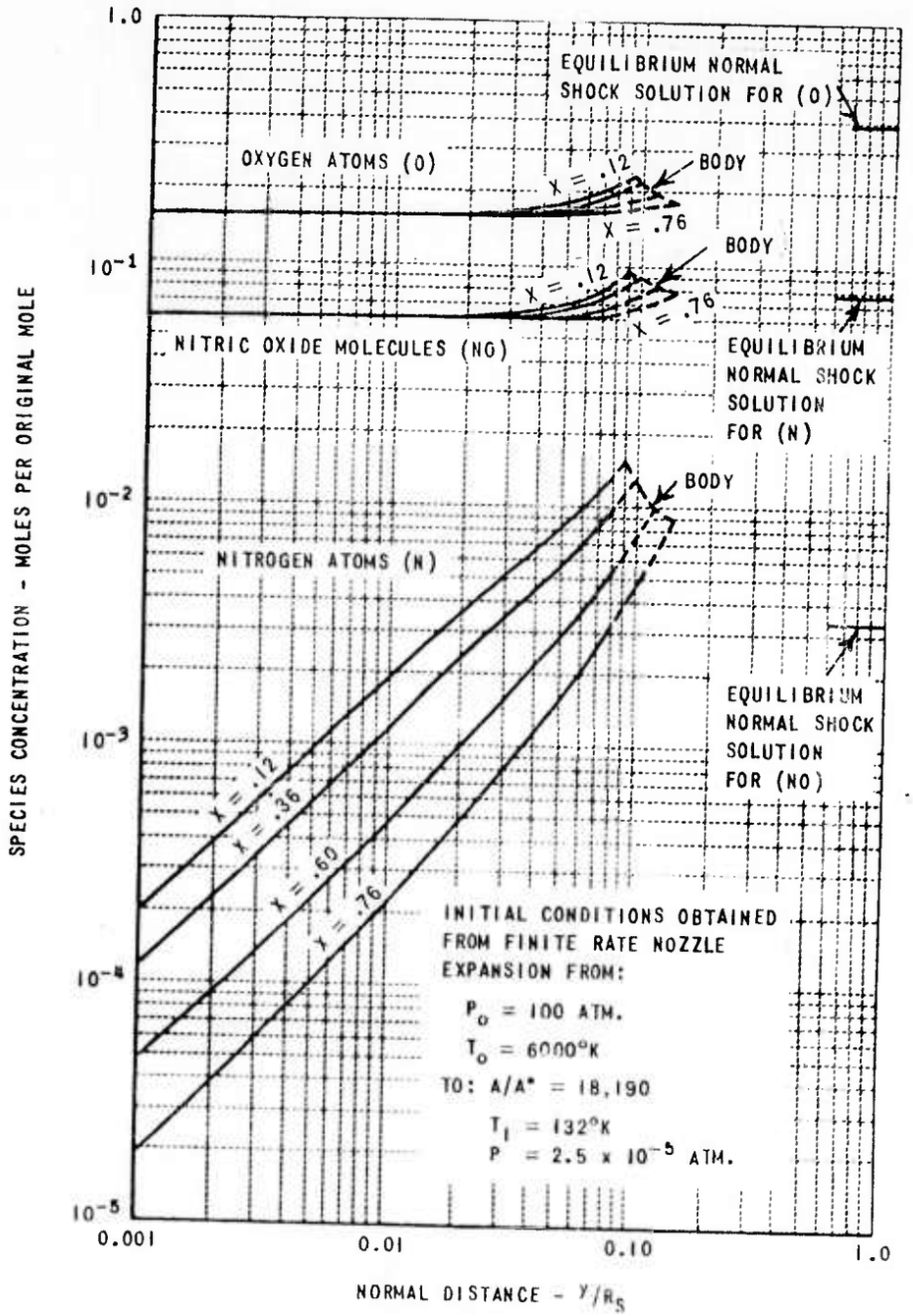

Figure 20 SPECIES CONCENTRATION AROUND NOSE OF HYPERSONIC VEHICLE

CATENARY SHOCK; 16.15 CM RADIUS AT CENTERLINE

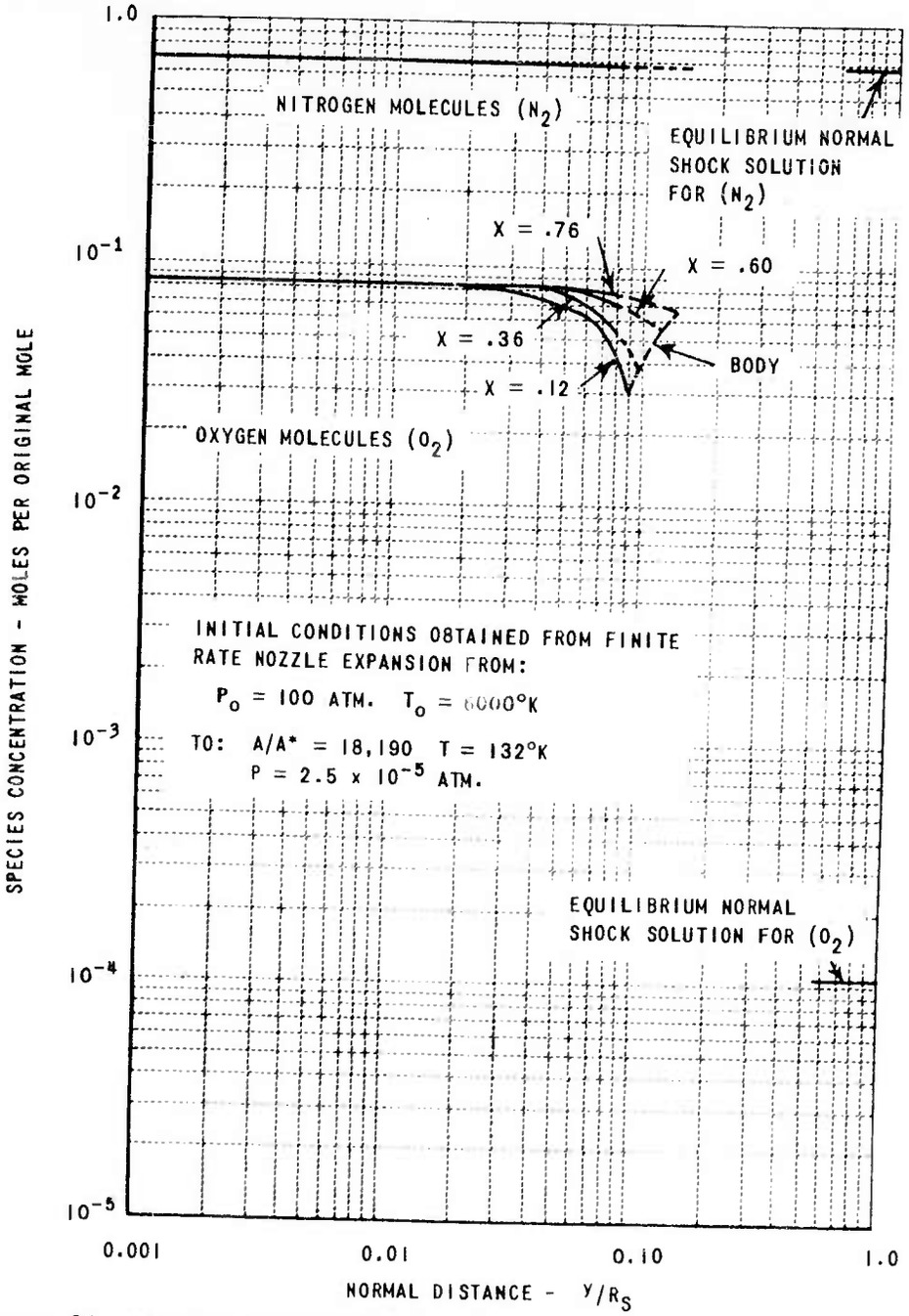

Figure 21 SPECIES CONCENTRATION AROUND NOSE OF HYPERSONIC VEHICLE

CATENARY SHOCK; 16.15 CM. RADIUS AT CENTERLINE

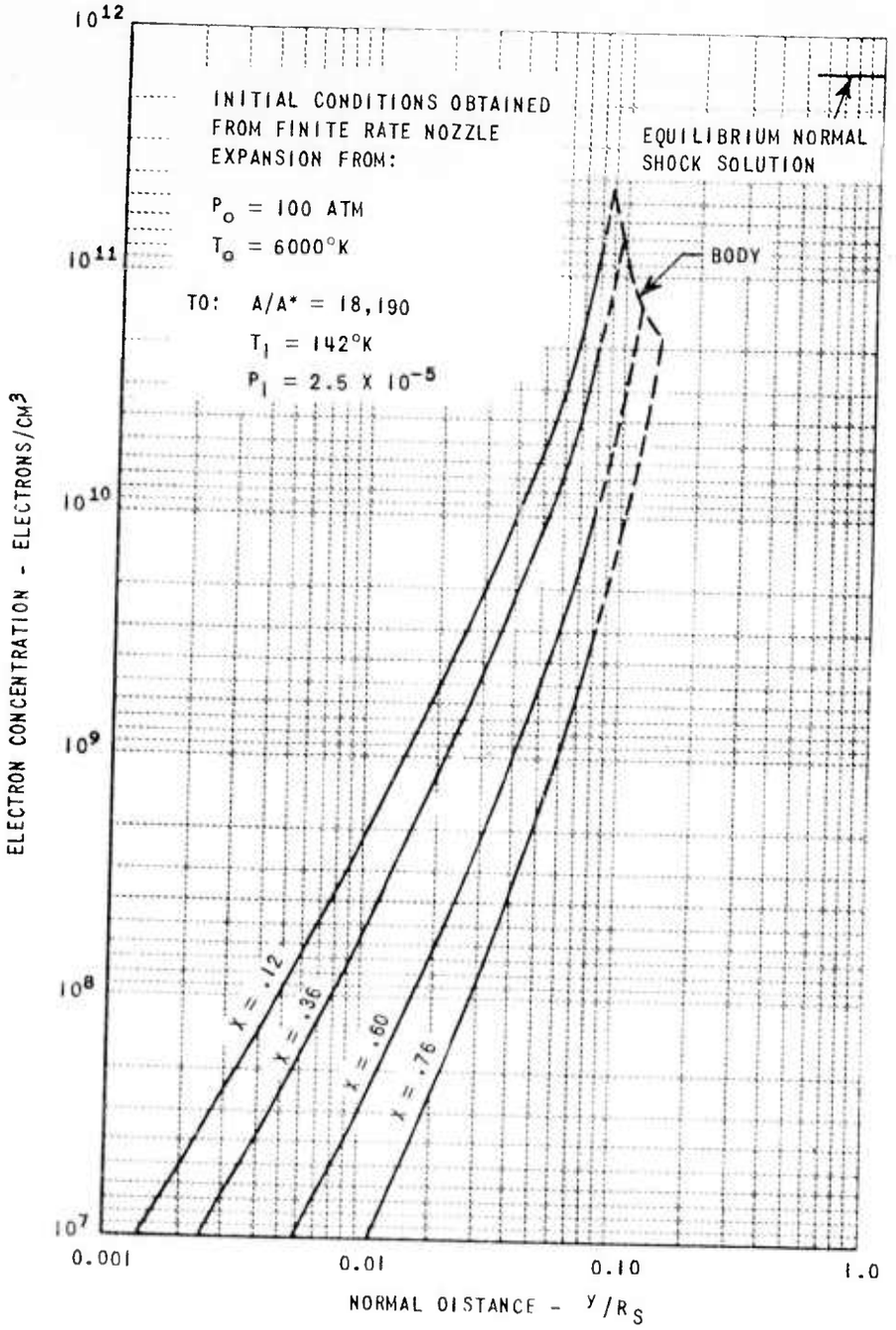

Figure 22 ELECTRON CONCENTRATION AROUND NOSE OF HYPERSONIC VEHICLE

CATENARY SHOCK; 16.15 CM RADIUS AT CENTERLINE

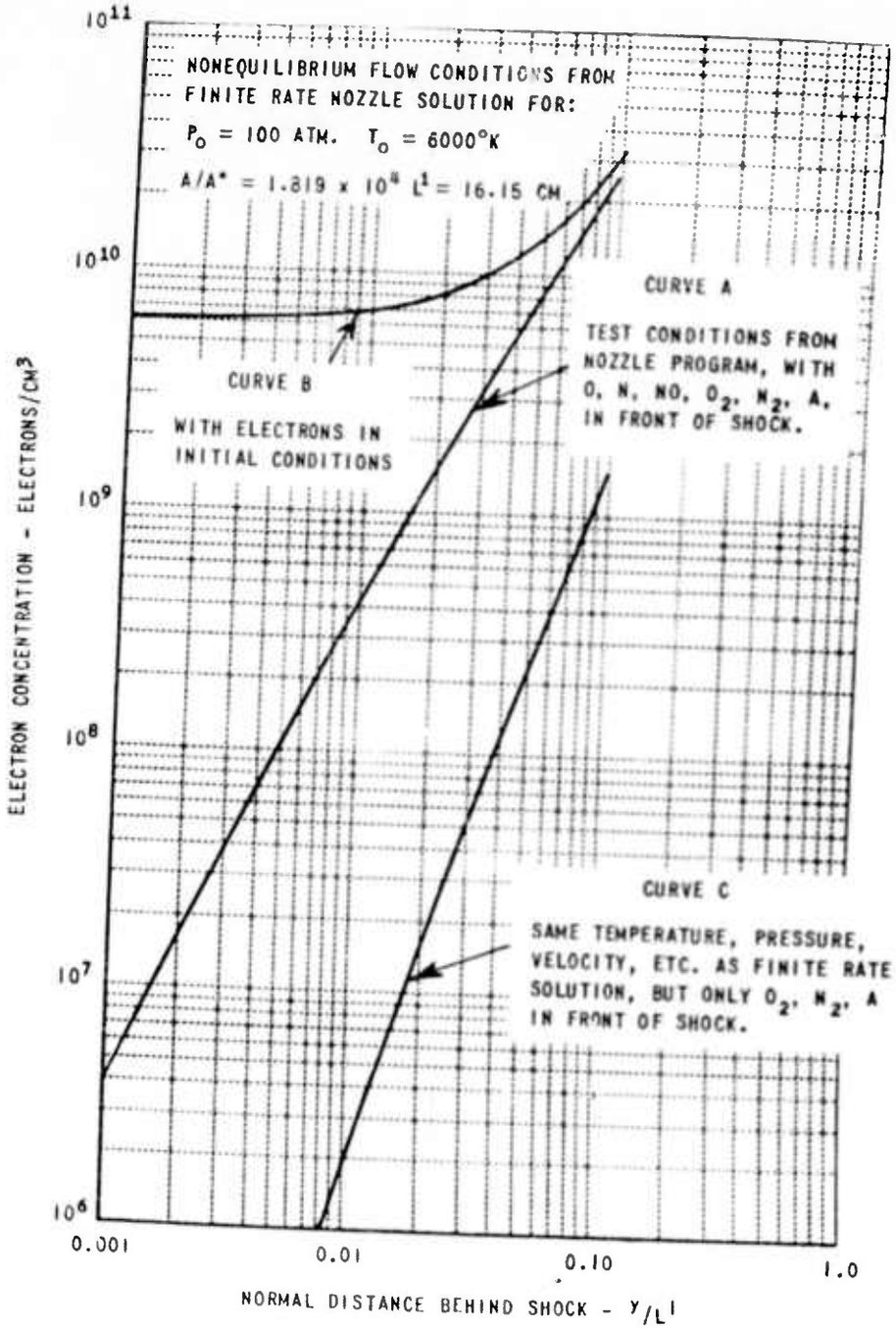

Figure 23 ELECTRON CONCENTRATION BEHIND NORMAL SHOCK WAVE IN DISSOCIATED AIR